Title

An Optimized RNF126-Targeting Covalent Handle for Molecular Glue Degraders

ISBN

9798189271694

Author

Modi, Aman Devare

Publication Date

2027-05-01

Peer reviewed|Thesis/dissertation

An Optimized RNF126-Targeting Covalent Handle for Molecular Glue Degraders

By

Aman Modi

A dissertation submitted in partial satisfaction of the
requirements for the degree of

Doctor of Philosophy

in

Chemistry

in the

Graduate Division

of the

University of California, Berkeley

Committee in charge:

Professor Daniel K. Nomura, Chair
Professor James Olzmann
Professor Ziyang Zhang

Spring 2026

Abstract

An Optimized RNF126-Targeting Covalent Handle for Molecular Glue Degraders

By Aman Modi

Doctor of Philosophy in Chemistry

University of California, Berkeley

Professor Daniel K. Nomura, Chair

One of the largest obstacles in modern drug discovery is that a significant portion (>90%) of the proteome is considered “undruggable,” in that these proteins lack a characterized, functional binding pocket or ligandable hotspot which small molecules can bind to and modulate the protein’s function for therapeutic benefit. To overcome such disease-causing proteins, targeted protein degradation (TPD) strategies have arisen, where the cell’s endogenous degradation machinery is hijacked to ubiquitinate and degrade the classically undruggable protein. Molecular glue degraders serve as a promising modality to achieve TPD. These are monovalent compounds that induce the proximity of a target protein with a component of the ubiquitin proteasome system to degrade the protein of interest. While our research group has previously identified a fumarate-based electrophilic handle that covalently modifies the E3 ligase RNF126 to enable degradation of multiple protein targets, the high intrinsic reactivity and cytotoxicity of the fumarate handle limited its translational utility.

This work describes the development of an optimized and metabolically stabilized RNF126-targeting covalent handle incorporating a *trans*-cyclobutane linker that exhibits reduced glutathione reactivity and diminished cytotoxicity while retaining robust degradative activity. Using BRD4 as a benchmark target, we demonstrate that this optimized handle yields a potent and selective BRD4 degrader whose activity is dependent on RNF126. We further extend this strategy to the androgen receptor (AR) and its clinically intractable splice variant AR-V7, demonstrating selective degradation of both AR and AR-V7 in androgen-independent prostate cancer cells and robust inhibition of AR transcriptional activity that surpasses the established AR antagonist enzalutamide.

Together, this dissertation establishes a generalizable, chemistry-centric framework for converting small-molecule ligands into covalent molecular glue degraders, offering a roadmap for exploiting event-driven pharmacology against the most intractable targets in the human proteome.

Table of Contents

Dedication

To Mom and Dad, thank you for your unwavering support throughout the past four years. To Ishu, thank you for being not just a brother, but a best friend and an anchor beyond science. Moving across the world, from Singapore to the U.K., and then to the U.S, has not always been easy. Having your support has made that journey possible and means the world to me.

To my friends, from Singapore to the U.K. to the Bay Area, thank you for standing by me through every stage of this process. I carry these friendships with me across every chapter, and they have enriched both my personal and professional life.

To Amy and Alyssa, it has been a privilege to mentor you and to watch you pursue careers in the sciences, and I am excited to see where your paths lead. To Emily, I look forward to your continued journey in the Nomura Lab; your dedication and curiosity will undoubtedly take you far.

To the Nomura Research Group, past and present, I am deeply grateful for both the scientific training and the friendships formed along the way. Ethan and Taylor, thank you for your friendship, both in and outside the lab, which has been a defining part of my time at Berkeley.

To Dan Nomura, thank you for your guidance and leadership over the past four years. You have created an environment that allowed me to grow as a scientist and realize my potential, and the experiences I've gained in this group are truly invaluable.

Acknowledgements

The work in chapter II was derived from a submitted bioRxiv manuscript with permission from the following co-authors: Ethan S. Toriki, Christian E. Stieger, Emily A. Lau, Claire Song, Alyssa Chew, Amy Tsao, Kaila Nishikawa, Jeffrey McKinna and Daniel K. Nomura. “An Optimized RNF126-Targeted Covalent Handle for Molecular Glue Degraders” was submitted to Bioorganic & Medicinal Chemistry Letters.

This work was also supported by Novartis Institutes for Biomedical Research and the Novartis-Berkeley Translational Chemical Biology Institute (NB-TCBI), the UC Berkeley Molecular Therapeutics Initiative (MTI), the Nomura Research Group and the Mark Foundation for Cancer Research ASPIRE Award.

We also thank Drs. Hasan Celik, and UC Berkeley’s NMR facility in the College of Chemistry (CoC-NMR) for spectroscopic assistance. Instruments in the College of Chemistry NMR facility are supported by in part by the NIH grant S10OD024998.

List of Figures

Abbreviations

13C NMR	Carbon-13 nuclear magnetic resonance
1H NMR	Proton nuclear magnetic resonance
ABPP	Activity-based protein profiling
ANOVA	Analysis of variant
AR	Androgen receptor
AR-V7	Androgen receptor splice variant 7
BET	Bromodomain and extra-terminal domain
BRD4	Bromodomain-containing protein 4
BSA	Bovine serum albumin
BTZ	Bortezomib
CDK4	Cyclin-dependent kinase 4
CETSA	Cellular thermal shift assay
CRBN	Cereblon
CuAAC	Copper-catalyzed alkyne-azide cycloaddition
DCAF11	DDB1- and CUL4-associated factor 11
DCAF16	DDB1- and CUL4-associated factor 16
DCM	Dichloromethane
DIPEA	Diisopropylethylamine
DMSO	Dimethyl sulfoxide
E3	Ubiquitin-protein ligase
ESI	Electrospray ionization
Et	Ethyl
EtOAC	Ethyl acetate
FAIMS	High-field asymmetric waveform ion mobiliy spectroscopy
FBXO22	F-box protein 22
FDR	False discovery rate
FEM1B	Fem-1 homolog B
GAPDH	Glyceraldehyde-3-phosphate dehydrogenase
GSH	Glutathione
GSPT1	G1 to S phase Transition 1
HATU	2-(1H-7-Azabenzotriazol-1-yl)-1,1,3,3-tetramethyluronium
HEK293T	Human embryonic kidney 293T cells

IA-rhodamine	Iodoacetamide-rhodamine
KO	Knockout
LC-MS/MS	Liquid chromatography-tandem mass spectrometry
NMR	Nuclear magnetic resonance
PROTAC	Proteolysis-targeting chimera
RNF4	RING finger protein 4
RNF114	RING finger protein 114
RNF126	RING finger protein 126
SAR	Structure-activity relationship
SDS-PAGE	Sodium dodecyl sulfate-polyacrylamide gel electrophoresis
TFA	Trifluoroacetic acid
TMT	Tandem mass tag
TPD	Targeted protein degradation
UPS	Ubiquitin-proteasome system
WT	Wild-type
VAV1	Proto-oncogene vav

I. Background on Covalent Drug Discovery and Targeted Protein Degradation

1.1 Covalent Drug Discovery

1.1.1 Reversible Inhibitors

Small molecule modulation of disease-causing proteins has been the predominant method of treating disease. While biologics and cell therapies are competing modalities, small molecules comprised over 70% of approved drugs in 2025, highlighting their importance in the therapeutic landscape1. Many proteins contain deep ‘pockets’, often hydrophobic clefts that small molecules and metabolites can bind to. Pathogenic proteins have predominantly been drugged through exploitation of such pockets. They engage these pockets reversibly, stabilized by non-covalent interactions between the small molecule and protein. Therefore, to drive strong inhibition of a target protein, these molecules need to engage a protein persistently, or else they will dissociate. For deep hydrophobic pockets, it has generally been possible to design molecules with high residence times and therefore a low dissociation constant (K_d) **(Figure 1.1a)**.

1.1.2 Covalent Inhibitors

Unfortunately, many disease-causing proteins do not possess these ligandable pockets. For proteins containing shallower pockets, covalent interactions may be required to drive longer residence times and faster on rates (k_{on}). As a result, covalent drugs have recent seen gains in popularity to address these proteins that have thus far been intractable to traditional small molecule inhibition. To facilitate this, many covalent ‘warheads’ have been developed, which are electrophiles that react selectively with a particular amino acid to form an irreversible interaction. Covalent drugs typically engage their targets in a stepwise manner. First, they form a drug-protein complex governed by non-covalent interactions, then the warhead reacts with a proximal amino acid to form the irreversible covalent bond. The observed rate of drug inhibition is defined as the k_{inact}/K_i ratio, where k_{inact} represents the warhead reactivity and K_i reflects the strength of the non-covalent protein-ligand interactions[2] **(Figure 1.1b)**. Therefore, even a relatively weak K_i can be compensated by high warhead reactivity, and thus weak binders that engage shallow protein pockets can be bolstered by addition of a covalent warhead. However, covalent pharmacology strategies must be deployed carefully, due to the risk of non-specific interactions that lead to off-target toxicities and reactivity with metabolites such as glutathione that consume the warhead. Recent advances have involved tuning covalent warheads such that they only react upon engagement of a target and do not react promiscuously with the entire proteome.

By far the most common amino acid target in covalent drug discovery is cysteine (C). Cysteine’s thiol is redox sensitive and nucleophilic, the latter of which is enhanced significantly in the thiolate form[4]. Cysteine bears a pK_a of 10, meaning under certain physiological conditions, such as involvement in an active site, the thiolate form my

dominate and be able to act as a potent nucleophile. The acrylamide has been the warhead of choice for covalent drug discovery, but a wide variety of warheads are now being explored **(Figure 1.1c)**. The flagship example of selective cysteine-reactive drugs was the development and eventual approval of Sotorasib, a selective KRAS G12C inhibitor that covalently engages the cysteine-bearing mutant form spares other KRAS types[3]. KRAS, one of the most sought-after oncology targets, was historically deemed undruggable due to an inability to outcompete GTP/GDP from its active site and the lack of other druggable pockets.

1.2 PROTACs as Targeted Protein Degradation Modalities

Targeted protein degradation (TPD) is an emerging therapeutic strategy whereby small molecules that use the cell's native degradation machinery to ubiquitinate and degrade a target protein. This modality was first explored via development of Proteolysis-Targeting Chimeras (PROTACs), which are heterobifunctional molecules comprising a target-binding ligand, a linker, and an E3 ligase-recruiting element to induce proximity-driven ubiquitination and proteasomal degradation of the target protein[5] (Figure 1.2a). Importantly, however, degraders have also revealed differential pharmacology that distinguishes them from conventional inhibitors. Because degraders eliminate the target protein entirely rather than merely occupying an active site, they can ablate non-enzymatic scaffolding functions that are impervious to catalytic inhibition. This principle has been demonstrated for Bruton's tyrosine kinase (BTK), where PROTAC-mediated degradation suppresses both the catalytic and scaffolding roles of BTK in B-cell receptor signaling, an outcome not achievable with covalent BTK inhibitors such as ibrutinib[6]. Similarly, degradation of interleukin-1 receptor–associated kinase 4 (IRAK4) eliminates its critical scaffolding function in Myddosome formation, providing anti-inflammatory efficacy that surpasses kinase inhibition alone[7]. Beyond scaffolding, degraders offer a strategy to overcome resistance mutations that render active-site inhibitors ineffective. In the context of the androgen receptor (AR), mutations in the ligand-binding domain confer resistance to antiandrogens such as enzalutamide, yet degraders that eliminate the full-length protein – or as explored in this dissertation, the truncated splice variant AR-V7 – can bypass these resistance mechanisms[8,9]. These examples underscore that targeted protein degradation is not merely a surrogate for inhibition but constitutes a mechanistically distinct pharmacological modality with unique therapeutic potential. While PROTACs have demonstrated broad utility, they present distinct pharmacological challenges such as high molecular weight, complex linker optimization, limited oral bioavailability, and the hook effect at elevated concentrations.

1.3 Molecular Glues as Targeted Protein Degradation Modalities

Molecular glue degraders offer a compelling alternative modality for TPD. These monovalent small molecules induce or stabilize protein–protein interactions between a target protein and a component of the ubiquitin–proteasome system (UPS), typically an E3 ubiquitin ligase, to promote target ubiquitination and subsequent proteasomal degradation[10] **(Figure 1.2b)**. Compared with PROTACs, molecular glue degraders offer several advantages, including reduced molecular weight, simplified pharmacology, and the potential to engage targets that lack protein targeting ligands.

Despite the clinical success of certain molecular glue degraders, the rational and systematic discovery of new molecular glue degraders has remained a significant challenge. The serendipitous origins of IMiD-based degraders underscore the difficulty: their degradative mechanism was discovered only retroactively, decades after their initial clinical use. Cyclosporin A (CsA) was among the earliest molecular glues discovered, which was found to have immunosuppressive effects. Schreiber and Crabtree later discovered that CsA and related molecule FK506 act as molecular glues, forming a ternary complex between Cyclophilin A and the phosphatase calcineurin **(Figure 1.3a)**. Similarly, thalidomide was approved as a morning sickness drug, but was later discovered to induce birth defects and was removed from the market. Later, it was discovered that thalidomide was a molecular glue degrader, forming a ternary complex between the E3 ligase CRBN, a substrate receptor of the CRL4 complex, and members of the Ikaros protein family (IKZF1/3). The congenital defects were down to be a result of SALL4 degradation, an important transcription factor involved in early embryonic development[11] **(Figure 1.3a)**. Analogs of thalidomide, known as IMiDs (Immunomodulatory Drugs) were subsequently developed, including lenalidomide and pomalidomide, where a glutarimide-based structure was key to recognize a shallow hydrophobic pocket on the E3 ligase[12]. Modifications to the glutarimide structure have been used to tune the target degradation space. For instance, small changes in the structure of lenalidomide led to the degradation of CK1α[13]. CRBN targets have typically been restricted to those bearing a ‘G-loop’ degron, a β-hairpin motif that forms important protein-protein contacts with CRBN. More recently, IMiD-based degraders have been used to degrade a greater range of proteins, including GSPT1, NEK7 and VAV1 – the latter being a target that does not contain a G-loop[14].

While CRBN-targeting degraders have seen some success, target-centric molecular glue discovery beyond CRBN-based degraders has remained largely empirical, with limited mechanistic or chemical design rules guiding its development.[10,15] Some examples of non-CRBN target-centric molecular glue discovery include the transformation of a CDK12 inhibitor, Roscovitine, to a Cyclin K degrader, CR8, via simple appendage of a pyridine moiety. Another example includes the development of BI-3082, a BCL6 degrader that only differs from its parent inhibitor by a dimethyl-piperidine group.

These degraders add validity to the notion that protein-targeting ligands can be converted to degraders by small chemical changes at the ligand's exit vector, recruiting components of the ubiquitin-proteasome pathway.

Recent efforts have begun to establish chemistry-centric frameworks for the rational design of molecular glue degraders. Our laboratory and others have introduced strategies in which covalent electrophilic handles are systematically appended to known protein-targeting ligands to identify degradative activity[15–19].

1.4 Covalent Strategies for Molecular Glue Degraders

1.4.1 Covalency to Recruit Novel E3 Ligases

Covalency can be a useful strategy for two main reasons: first, E3 ligases are often considered 'undruggable' due to lack of ligandable pockets and therefore may require covalency for meaningful engagement. Second, irreversible engagement of an E3 ligase with a covalent compound can increase the lifetime of a ternary complex. Through chemoproteomic profiling, we previously identified permissive E3 ligase–target pairs and demonstrated that a fumarate-based electrophile could covalently engage the E3 ligase RNF126, thereby converting otherwise non-degradative inhibitors into molecular glue degraders of their respective targets[15].

The work described in this dissertation builds on a growing body of literature establishing covalent engagement of E3 ligase cysteines as a general strategy for molecular glue degrader discovery. In addition to RNF126, our laboratory has identified multiple covalent degradative handles that act through DCAF16 by selectively targeting C119 or a second cysteine cluster encompassing C173/C178[16–18]. These studies demonstrated that molecular glue degradation can be achieved by engaging distinct cysteine sites within the same E3 ligase and that productive degradation is governed not simply by covalent binding, but by the precise spatial and chemical compatibility between the electrophilic handle, the E3 ligase surface, and the recruited target protein **(Figure 1.4a)**.

Work from the Gray, Fischer, and Winter laboratories further established the importance of DCAF16 as a permissive E3 ligase for covalent molecular glue degraders, particularly through engagement of C58, in the context of BRD4 degradation, in addition to highlighting the significance of additional E3 ligases, including DCAF11 and FBXO22[18,18,20,21] **(Figure 1.4b)**. Collectively, these studies extend the original work on covalent targeting of DCAF16 and work by our laboratory in targeting RNF114 and RNF4 using electrophilic handles to enable targeted protein degradation[22–24].

1.4.2. Covalent Destabilizing Degraders

While conventional molecular glues and PROTACs involve recruitment of an E3 ligase to a protein of interest, the design of monovalent destabilizing degraders has also been

established. The Crews Lab demonstrated this by addition in a HaloTag-engineered system, using a small molecule with hydrophobic tags such as an adamantyl group to induce destabilization and subsequent proteasomal degradation[25]. However, these compounds are bifunctional molecules that require a genetically introduced fusion protein.

Recently, covalency has been used as a tool to induce protein destabilization by forming adducts with residues that govern folding or localization. Research from our group identified EN4, which engages a cysteine in an intrinsically disordered region of the proto-oncogene Myc. Furthermore, treatment with this compound resulted in thermal destabilization of the protein. This phenomenon was monitored using CETSA [26](Cellular Thermal Shift Assay). Typically, small molecule inhibition of an orthosteric pocket leads to protein stabilization, making this observation somewhat unique and points to a new pharmacology that may be generalizable. Our group has since developed selective destabilizing degraders for several targets, including β-Catenin[27], and IRF8 [28]and AR-V7[9] – all of which are therapeutically valuable intrinsically disordered transcription factors that have thus far evaded small molecule blockade. This provides the rationale for covalent destabilizing degraders to be a useful tool in addressing these targets.

1.5 Optimizing Covalent Handles for Translational Utility

The convergence of these independent efforts highlights a unifying principle for molecular glue degrader discovery: covalent engagement of E3 ligase cysteines represents a powerful and generalizable strategy for enabling degradation, but success hinges on treating the electrophilic handle as an optimizable chemical module rather than a fixed warhead. Our initial RNF126-targeting fumarate handle, while conceptually transformative, exhibited high intrinsic reactivity, rapid glutathione metabolism, and dose-limiting cytotoxicity that constrained its translational potential.

This dissertation addresses these limitations by describing the development of an optimized, second-generation RNF126-targeting covalent handle. By refining the electrophilic geometry and linker composition, we demonstrate that the liabilities of highly reactive covalent handles can be mitigated through chemical optimization without sacrificing degradative potency or selectivity. Chapter 2 presents the design, synthesis, and biological characterization of this optimized handle, including its application to both BRD4 and the androgen receptor system. Chapter 3 offers concluding remarks and future perspectives for the field.

1.6 Figures

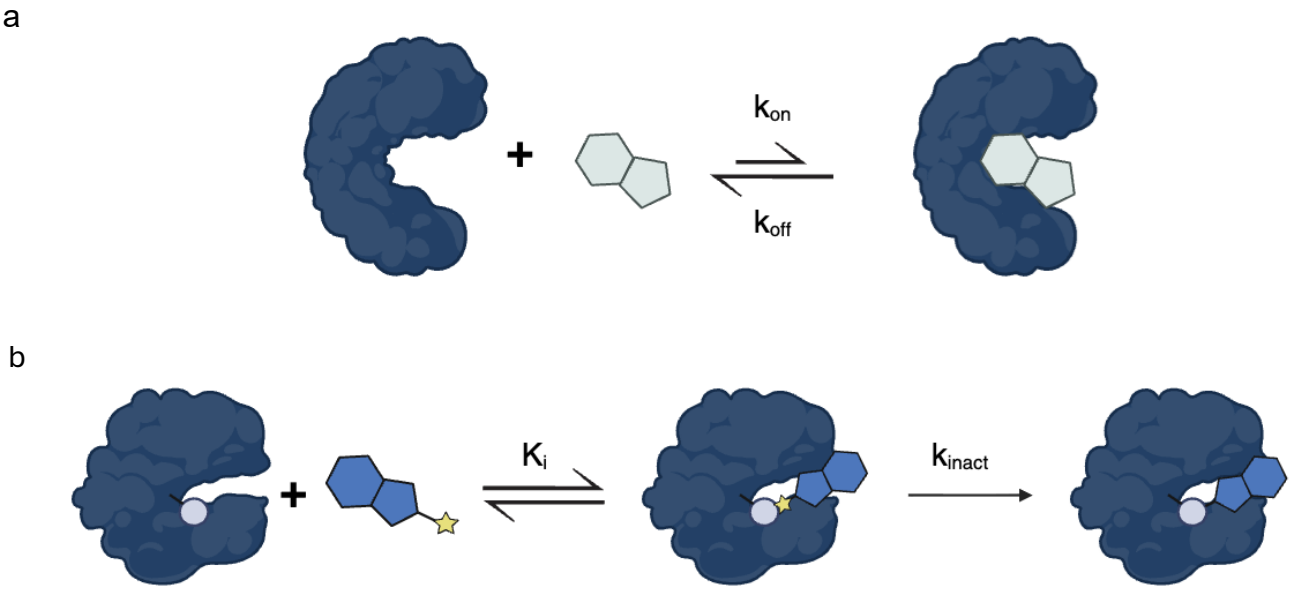

Figure 1.1 Covalent Drug Discovery Principles. a) Reversible binding is facilitated by non-covalent interactions, and K_d is calculated by the ratio of k_{off} to k_{on}. b) Covalent inhibition occurs via i) reversible binding and ii) irreversible warhead reactivity, forming a covalent adduct. c) Examples of covalent warheads, targeting cysteine, lysine, serine and aspartic acid.

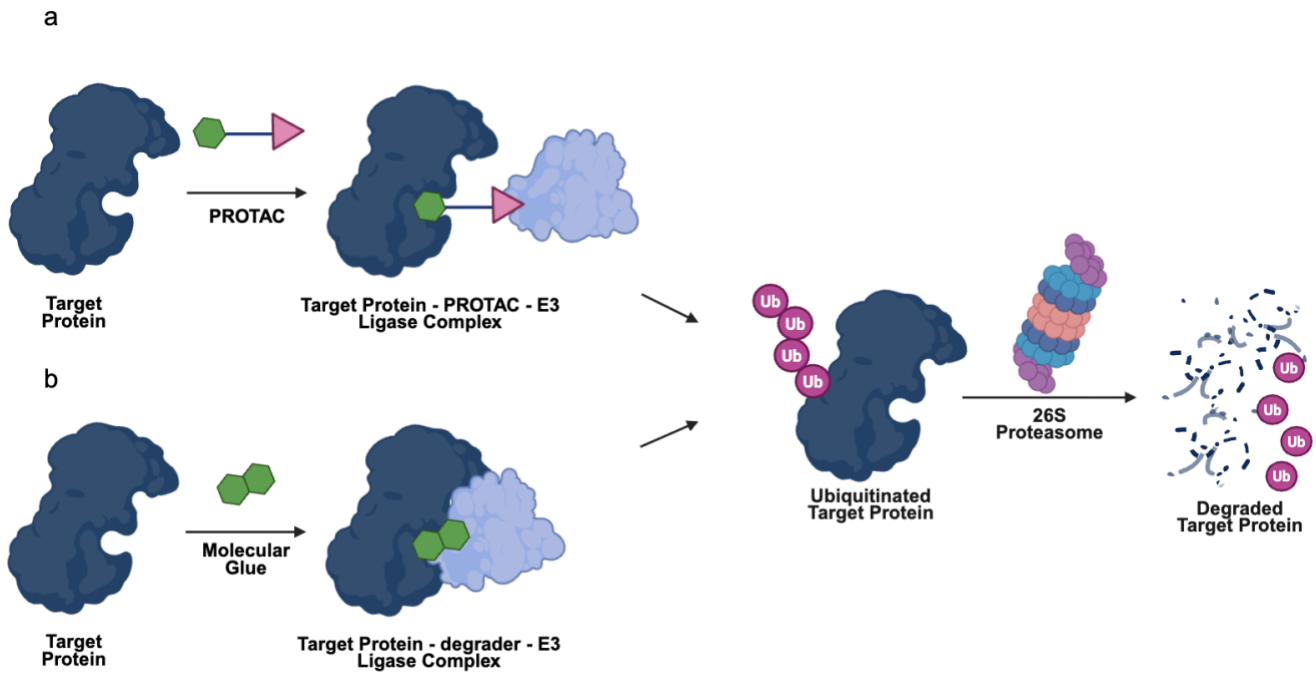

Figure 1.2 Targeted Protein Degradation using Molecular Glue Degraders and PROTACs. a) Heterobifunctional molecules induce proximity between a protein of interest and E3 ligase complex. The short-lived ternary complex is polyubiquitinated, resulting in recruitment to 26S proteasome and eventual degradation. b) Monovalent degraders bind cooperatively to the target protein and E3 ligase, facilitating productive protein-protein interactions. Subsequent ubiquitination leads to degradation of the protein of interest.

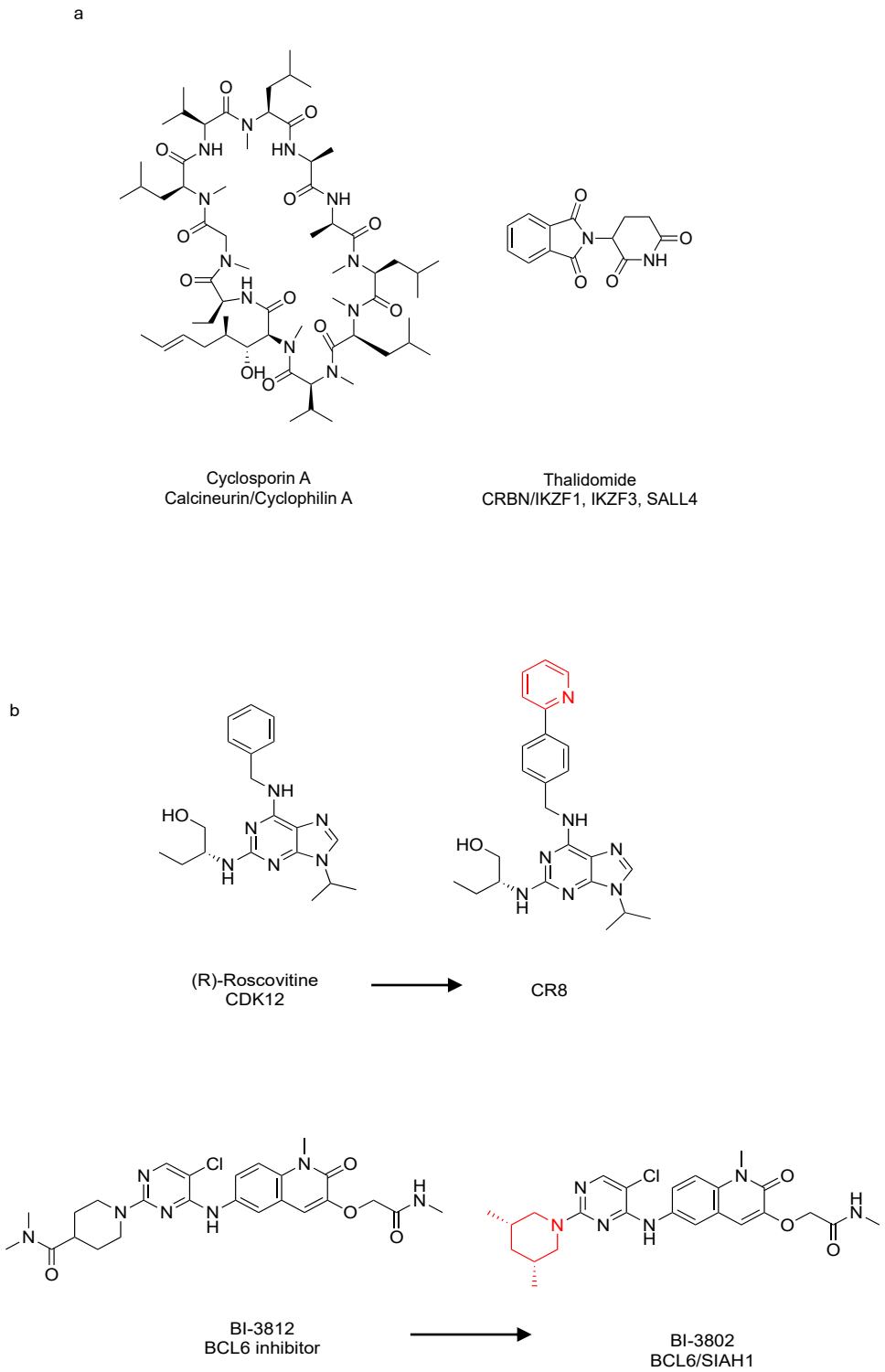

Figure 1.3 Examples of Molecular Glue Degraders. a) Early molecular glue degraders were discovered serendipitously, such as cyclosporin A and thalidomide. b) Target-centric design of molecular glue degraders. CR8 was developed by appendage of pyridine to

Roscovitine to degrade Cyclin K, and BI-3801 was converted to BCL6 degrader BI-3802 through addition di-methylpiperidine

a

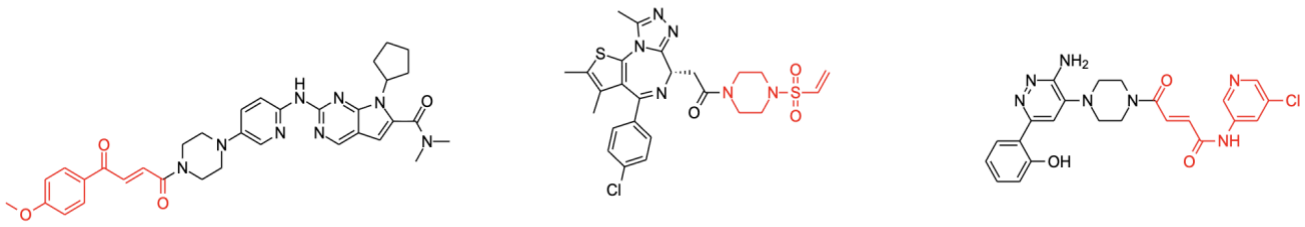

EST1060

CDK4 degrader

RNF126 C32

ML-1-50

BRD4 degrader

DCAF16 C119

LO-3-61

BRD4 degrader

DCAF16 C173/178

b

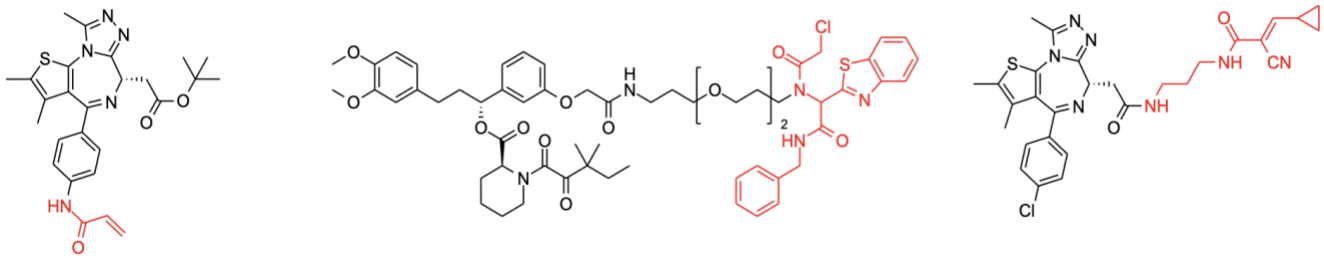

MMH1

BRD4 degrader

DCAF16 C58

22-SLF

FKBP12 degrader

FBXO22 C227/228

RCS-03-104-4

BRD4 degrader

DCAF11

Figure 1.4 Examples of Cysteine Reactive Molecular Glue Degraders. a) Covalent molecular glues discovered by our group, including RNF126 and DCAF16-mediated degraders. b) Other examples of cysteine-engaging covalent molecular glue degraders.

II. Design of Optimized RNF126-targeted Covalent Handle for Degradation of BRD4 and AR-V7

This chapter is based on the bioRxiv preprint “An Optimized RNF126-Targeting Covalent Handle for Molecular Glue Degraders[29]” and has been adapted with permission from all co-authors

2.1 Summary

Molecular glue degraders represent a powerful modality for targeting proteins that are refractory to traditional inhibition. However, rational design principles for molecular glue degraders remain poorly defined. Previously, we reported a chemistry-centric strategy to identify covalent degradative handles that, when appended to established ligands, convert non-degradative inhibitors into molecular glue degraders by engaging permissive E3 ligases. This effort identified a fumarate-based electrophilic handle that covalently modified the E3 ligase RNF126, enabling degradation of multiple protein targets when transplanted across diverse ligands. Despite its conceptual impact, the high intrinsic reactivity and cytotoxicity of the fumarate handle limited its translational utility. Here, we report the development of an optimized and metabolically stabilized RNF126-targeting covalent handle incorporating a *trans*-cyclobutane linker that exhibits reduced glutathione reactivity and diminished cytotoxicity while retaining robust degradative activity. When appended to the BET bromodomain inhibitor JQ1, this optimized handle yielded a potent and selective BRD4 degrader whose activity was dependent on RNF126. Importantly, transplantation of this handle onto a previously non-inhibitory ligand targeting the androgen receptor (AR) and its truncation variant, AR-V7, enabled selective degradation of both AR and AR-V7 in androgen-independent prostate cancer cells, thereby robustly inhibiting AR transcriptional activity beyond the established AR antagonist enzalutamide. Collectively, these findings demonstrate an optimized RNF126-based covalent handle for the rational development of molecular glue degraders against transcriptional regulators, including undruggable variants such as AR-V7.

2.2 Introduction

Targeted protein degradation has emerged as a transformative approach for modulating protein function beyond the limits of classical inhibition[10]. While heterobifunctional degraders such as Proteolysis Targeting Chimeras (PROTACs) have demonstrated broad utility, molecular glue degraders offer distinct advantages, including reduced molecular weight, simplified pharmacology, and the potential to engage proteins lacking ligandable pockets and targeted-chemical matter[5]. Despite notable clinical and preclinical successes, target-centric molecular glue discovery beyond CRBN-based degraders remains largely empirical, with limited mechanistic or chemical design rules guiding its development[10].

We and others have recently introduced chemistry-centric strategies for molecular glue discovery in which covalent electrophilic handles were systematically appended to known ligands to identify degradative activity[15–19]. Using chemoproteomic profiling, we previously identified permissive E3 ligase–target pairs and demonstrated that a fumarate-based electrophile could covalently engage the E3 ligase RNF126, thereby converting otherwise non-degradative inhibitors into molecular glue degraders of their respective targets.[4] This work provided a generalizable framework for molecular glue design by

decoupling target binding from E3 ligase engagement. However, the fumarate electrophile used in this initial study exhibited high intrinsic reactivity, rapid glutathione consumption, and dose-limiting cytotoxicity, collectively constraining its translational potential. We hypothesized that refining the warhead reactivity and linker topology of the RNF126-targeting handle would preserve productive engagement of RNF126 while improving metabolic stability and cellular tolerability.

Here, we report the development of a next-generation RNF126-targeting covalent handle incorporating a *trans*-cyclobutane linker that reduces electrophile reactivity while maintaining RNF126 engagement. Using BRD4 as a benchmark target, we demonstrated that this optimized handle enabled potent, selective, and RNF126-dependent degradation with minimal cytotoxicity. We further extended this strategy to androgen receptor (AR) biology, generating a molecular glue degrader capable of eliminating both full-length AR and the clinically intractable splice variant AR-V7, which lacks the ligand-binding domain and drives resistance to current therapies in prostate cancer. Together, these studies established an optimized chemical blueprint for RNF126-based molecular glue degraders and demonstrated their utility against a transcription factor previously considered undruggable.

2.3 Results

2.3.1 Optimization of an RNF126-Targeting Covalent Handle for BRD4 Degradation

We first evaluated the degradative activity and liabilities of the original fumarate-based BRD4 degrader JP-2-197 **(Figure 2.1a).** Treatment of HEK293T cells with JP-2-197 led to robust degradation of both long and short BRD4 isoforms in RNF126 wild-type cells but not in RNF126 knockout cells, confirming strict RNF126 dependence **(Figure 2.1b-2.1c).** However, JP-2-197 exhibited rapid glutathione reactivity (GSH $t_{1/2}$ = 29 min) and pronounced cytotoxicity at higher concentrations **(Figure 2.1a, 2,1d),** underscoring the need for a less reactive and less cytotoxic alternative.

To address these limitations, we designed a second-generation RNF126-targeting handle incorporating a *trans*-cyclobutane linker, yielding the BRD4 degrader J594 **(Figure 2.2a).** This modification substantially improved glutathione stability (GSH $t_{1/2}$ = 68 min) while preserving the covalent engagement of the pure RNF126 protein, as demonstrated by gel-based activity-based protein profiling [9], which showed competition for rhodamine-functionalized iodoacetamide (IA-rhodamine) labeling **(Figure 2.2b).** We further demonstrated cellular RNF126 engagement and enrichment with an alkyne-functionalized version of our optimized RNF126 handle, EST2002, without enrichment of an unrelated protein, vinculin **(Figure 2.2c-2.2d)**. Importantly, J594 induced dose-dependent degradation of BRD4 with minimal effects on cell viability across the tested concentration range **(Figure 2.2e-2.2f).**

We next confirmed the RNF126 dependence and BRD4 degradation selectivity mediated by J594 (Figure 3a-3b). We showed that the BRD4 degradation observed upon J594 treatment in RNF126 wild-type HEK293T cells was significantly attenuated in RNF126 knockout cells (Figure 3a-3b). We observed near-complete, but not complete, rescue of BRD4 degradation in knockout cells, potentially indicating that additional E3 ligases may be involved (Figure 3a-3b). Quantitative proteomic analysis further demonstrated that BRD4 was the dominant protein significantly downregulated following J594 treatment, indicating high target selectivity and minimal off-target effects (Figure 3c). These results established that the optimized RNF126-targeting handle maintains the defining features of the original fumarate scaffold—potent and selective molecular glue-mediated degradation—while substantially improving metabolic and cellular tolerability.

2.3.2 Transplantation of the Optimized Handle Enables Degradation of AR and AR-V7

Having validated the optimized handle through observing BRD4 degradation, we next sought to test whether this handle could be transplanted onto a ligand targeting the AR and its splice variant AR-V7. AR-V7 lacks the ligand-binding domain targeted by approved AR antagonists and is a key driver of resistance in androgen-independent prostate cancer[30,31]. Although AR antagonists and AR PROTACs are in clinical use or in clinical development[32,33], these molecules all target the ligand-binding domain and are ineffective against AR-V7. AR-V7 is considered undruggable since the remaining N-terminal and DNA-binding domains are largely unstructured and intrinsically disordered[30,31]. While our lab has previously identified a direct-acting, selective, covalent destabilizing degrader that targets the intrinsically disordered C125 on AR and AR-V7, this degrader is not potent and is stoichiometric due to its covalent engagement with the target protein[9]. A molecular glue degrader with reversible AR-V7 targeting would be more desirable for enabling sub-stoichiometric and catalytic degradation of the target[5].

We synthesized the AR/AR-V7 degrader EST1140 by appending the optimized RNF126-targeting handle to VPC-14228 [34,35]**(Figure 2.4a).** While this ligand has been previously shown to bind to the DNA-binding domain of AR and act as a functional antagonist of AR transcriptional activity, promoting its use in the development of PROTACs, in our hands, VPC-14228 does not inhibit, but instead stimulates AR transcriptional activity in 22Rv1 prostate cancer cells expressing AR and AR-V7 **(Figure 2.5a)**. We have also shown that previously disclosed PROTACs using this ligand do not degrade AR or AR-V7[15]. In contrast, we demonstrated that our original RNF126-based fumarate handle was capable of degrading AR and AR-V7, although it was also cytotoxic and did not exhibit the desired selectivity[15]. Nonetheless, to further confirm that VPC-14228 engages AR and AR-V7 in cells, we synthesized an alkyne-

functionalized photoaffinity probe based on VPC-14228 and demonstrated that this probe could be used to engage and enrich AR and AR-V7 in 22Rv1 cells **(Figure 2.5c-2.5d).** We appended our optimized fumarate handle onto VPC-14228 to generate EST1140. We demonstrated that EST1140 still covalently bound to pure RNF126 protein, as demonstrated by competition with IA-rhodamine labeling **(Figure 2.4b).** EST1140 treatment in 22Rv1 prostate cancer cells, which express both AR and AR-V7, led to a dose- and proteasome-dependent degradation of both proteins **(Figure 2.4c-2.4d).** We further demonstrate that the covalent handle was necessary for this degradation as a non-reactive derivative AM-2-040 was incapable of degrading AR and AR-V7 **(Figure 2.5e-2.5f).** These data contrasted with the clinically approved prostate cancer AR antagonist enzalutamide, which does not alter AR or AR-V7 levels, and with the ARV110 PROTAC under clinical development, which eliminates only full-length AR, not AR-V7 **(Figure 2.4e)**. Quantitative proteomics revealed highly selective degradation of AR/AR-V7 with minimal off-target effects **(Figure 2.4f).** Importantly, EST1140-mediated degradation of FLAG-tagged AR was abrogated in RNF126 knockout cells, establishing RNF126 dependence **(Figure 2.4g-2.4h).**

2.3.3 EST1140 Disrupts AR and AR-V7 Stability and Suppresses AR Transcriptional Activity

To further assess AR and AR-V7 target engagement by EST1140 and the functional consequences of AR/AR-V7 degradation, we performed cellular thermal shift assays (CETSA) in 22Rv1 cells [36]. Interestingly, while EST1140 does not covalently engage AR or AR-V7, EST1140 treatment significantly destabilized both AR and AR-V7, resulting in marked reductions in thermal stability relative to control conditions **(Figure 2.6a-2.6b).** First, this CETSA-based destabilization confirmed that EST1140 engaged AR and AR-V7 in 22Rv1 cells. Second, these data suggest that EST1140 degrades these proteins not only via RNF126-dependent molecular glue degrader mechanisms but also through the destabilization of AR and AR-V7. These data were reminiscent of our recently disclosed covalent destabilizing degrader of AR and AR-V7, EN1441, which acts by covalently modifying C125 on AR/AR-V7 [37]. Functionally, EST1140 robustly inhibited AR-dependent transcriptional activity with an EC_{50} of approximately 8 μM, compared to enzalutamide, which only showed a partial inhibition of total AR transcriptional activity in 22Rv1 cells, with less than 50 % inhibition at even the highest concentrations, since enzalutamide does not bind to AR-V7 **(Figure 2.6c-2.6d).** These findings demonstrated that RNF126-based molecular glue degradation provides a distinct and more effective mechanism for suppressing AR transcriptional activity in androgen-independent prostate cancer cells.

2.4 Discussion

This study advances molecular glue degrader design by demonstrating that the liabilities of highly reactive covalent handles can be mitigated through chemical optimization without sacrificing degradative potency or selectivity. By refining the geometry and linker composition of a fumarate-based RNF126-targeting electrophile, we developed a second-generation covalent handle with improved glutathione stability, reduced cytotoxicity, and preserved E3 ligase engagement.

Using BRD4 as a benchmark, we showed that this optimized handle supports potent, selective, and RNF126-dependent degradation with minimal off-target effects. Importantly, the modularity of this handle enabled its transplantation onto a previously non-functional AR-V7 ligand, yielding a molecular glue degrader capable of eliminating both full-length AR and the classically undruggable AR-V7 variant. This capability addresses a major unmet need in prostate cancer therapy, where resistance driven by AR-V7 remains a significant challenge.

The work described here builds on our and others' prior efforts to establish a chemistry-centric framework for the rational design of molecular glue degraders via covalent engagement of E3 ligases [15–19]. In addition to RNF126, we have previously identified multiple covalent degradative handles that act through DCAF16 by selectively targeting C119 or a second cysteine cluster encompassing C173/C178 [16,17]. These studies demonstrated that molecular glue degradation can be achieved by engaging distinct cysteine sites within the same E3 ligase and that productive degradation is governed not simply by covalent binding per se, but by the precise spatial and chemical compatibility between the electrophilic handle, the E3 ligase surface, and the recruited target protein. Work from the Gray, Fischer, and Winter laboratories further established the importance of DCAF16 as a permissive E3 ligase for covalent molecular glue degraders, particularly through engagement of C58, in the context of BRD4 degradation, in addition to highlighting the significance of additional E3 ligases, including DCAF11 and FBXO22 [18–21]. Collectively, these studies also extend the original work by Cravatt and Zhang on covalent targeting of DCAF16 and work by our lab in targeting RNF114 and RNF4 using electrophilic handles to enable targeted protein degradation [22–24].

Importantly, the convergence of these independent efforts highlights a unifying principle for molecular glue degrader discovery: covalent engagement of E3 ligase cysteines represents a powerful and generalizable strategy for enabling degradation, but success hinges on treating the electrophilic handle as an optimizable chemical module rather than a fixed warhead. By demonstrating that an optimized RNF126-targeting handle can be transplanted across structurally and biologically distinct targets – including the transcription factor variant AR-V7 – this work extends the scope of covalent molecular glue degraders beyond classically druggable targets such as BET

proteins and kinases. It reinforces the value of a modular, handle-centric design paradigm.

Future efforts will focus on expanding the scope of RNF126-based molecular glues, further tuning electrophile reactivity for in vivo applications, and exploring the generalizability of this approach across additional E3 ligases and disease-relevant targets. Beyond RNF126, RNF4, DCAF16, FBXO22, DCAF11, and FEM1B [16,17,19,20,22,23], future efforts will focus on identifying new covalent degradative handles and permissive E3 ligase pairs that can be harnessed for the rational design of molecular glue degraders. Taken together, this work provides both a practical molecular glue scaffold and a conceptual framework for advancing covalent molecular glue degraders toward therapeutic development.

2.5 Figures

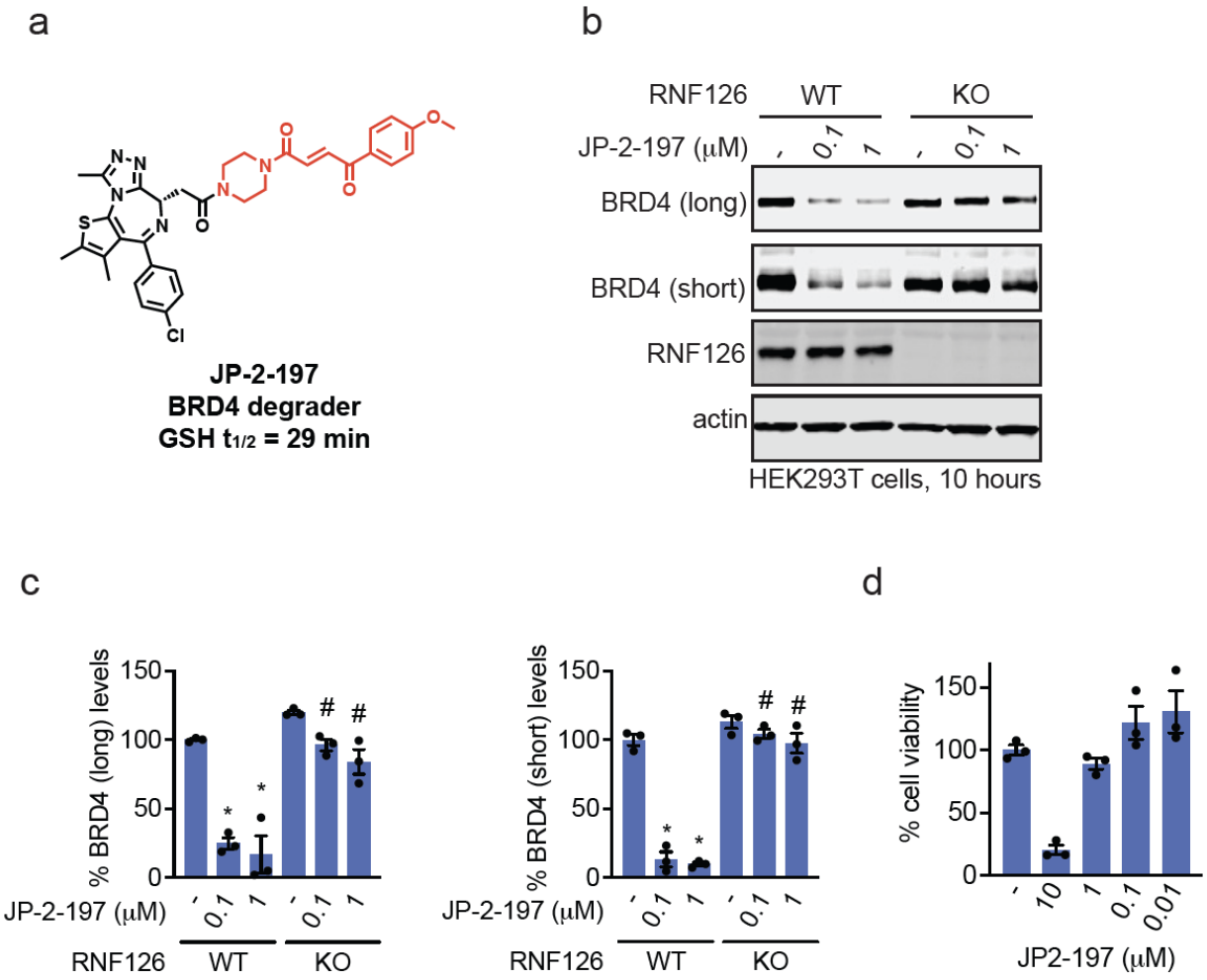

Figure 2.1 Characterization of the original fumarate-based RNF126-dependent BRD4 degrader JP-2-197. (a) Chemical structure of JP-2-197 and glutathione half-life. **(b)** BRD4 degradation in HEK293T cells. RNF126 wild-type (WT) and knockout (KO) cells were treated with DMSO vehicle or JP-2-197 for 10 h, after which BRD4, RNF126, and loading control actin levels were assessed by SDS/PAGE and Western blotting. **(c)** Quantification of BRD4 and RNF126 protein levels from **(c)**. **(d)** HEK293T cell viability. HEK293T cells were treated with DMSO vehicle or JP-2-197 for 24 h, after which cell viability was assessed by CellTiter-Glo. Blot in **(b)** is representative of n=3 biologically independent replicates per group. Bar graphs in **(c,d)** show individual replicates and

average ± sem. Significance in **(c)** expressed as *p<0.05 compared to vehicle-treated WT control and #p<0.05 compared to respective concentrations of WT conditions.

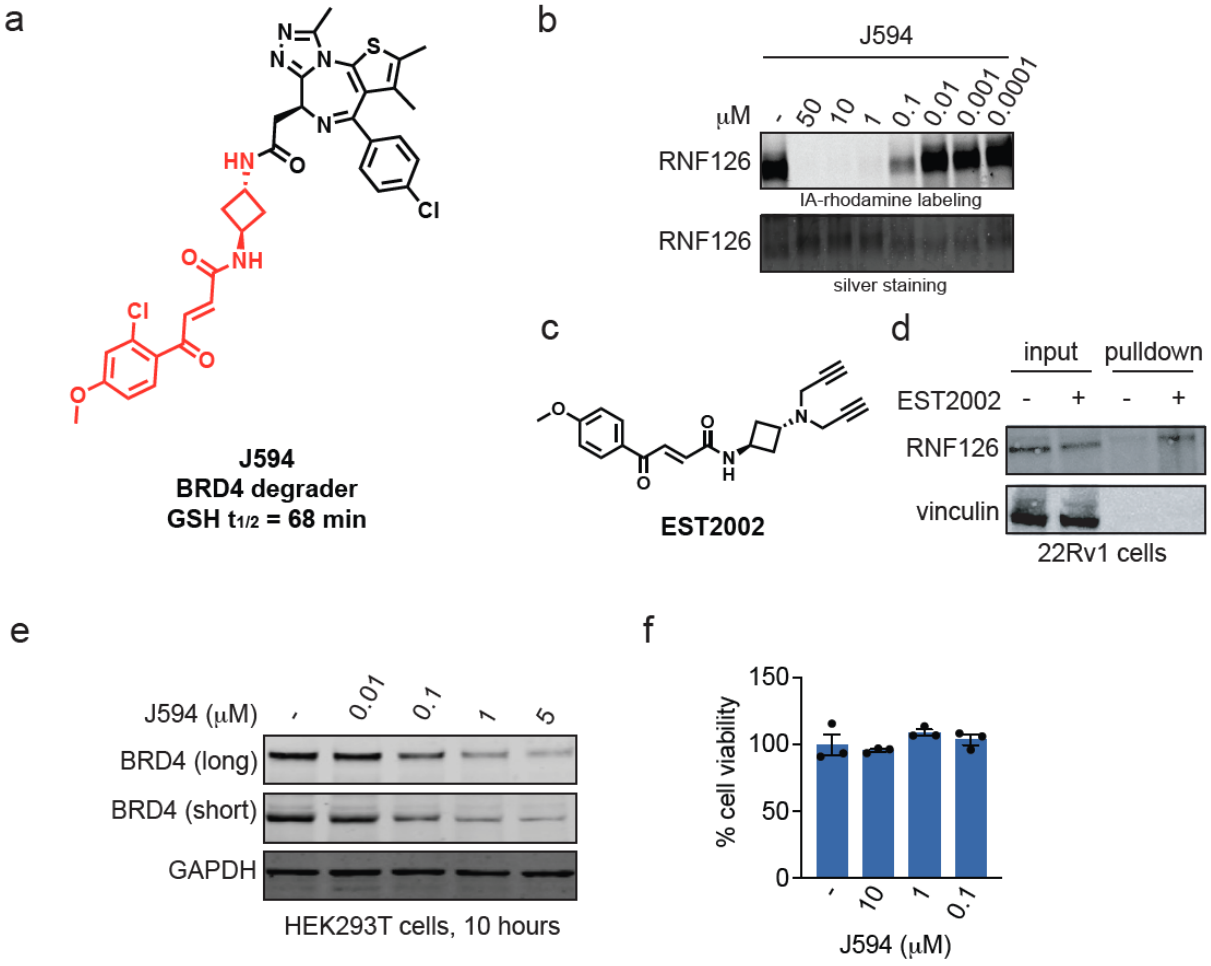

Figure 2.2 Development of an optimized RNF126-targeting BRD4 degrader. (a) Chemical structure of J594 with improved glutathione stability. **(b)** Gel-based ABPP of J594. RNF126 pure protein was pre-incubated with DMSO vehicle or J594 for 30 min prior to incubation with IA-rhodamine (100 nM) for 1 h, after which proteins were

separated by SDS/PAGE and visualized by in-gel fluorescence. Loading was assessed by silver staining. **(c)** Structure of alkyne-functionalized RNF126 handle, EST2002. **(d)** RNF126 target engagement in cells. 22Rv1 cells were treated with DMSO vehicle or EST2002 (10 μM, 2 h), after which proteomes were subjected to copper-catalyzed alkyne-azide cycloaddition (CuAAC) with a biotin-functionalized azide enrichment handle, probe-labeled proteins were avidin-enriched, and eluted. Input proteome and pulldown proteins were separated by SDS/PAGE, and RNF126 and unrelated negative control protein vinculin were visualized by Western blotting. **(e)** Dose-response of BRD4 degradation. HEK293T cells were treated with DMSO vehicle or J594 for 10 h, after which BRD4 and loading control GAPDH levels were assessed by SDS/PAGE and Western blotting. **(f)** Cell viability following J594 treatment. HEK293T cells were treated with DMSO vehicle or J594 for 24 h, after which cell viability was assessed by CellTiter-Glo. Blots in **(b,d,e)** are representative of n=3 biologically independent replicates per group. Data in **(f)** shows individual replicates and average ± sem.

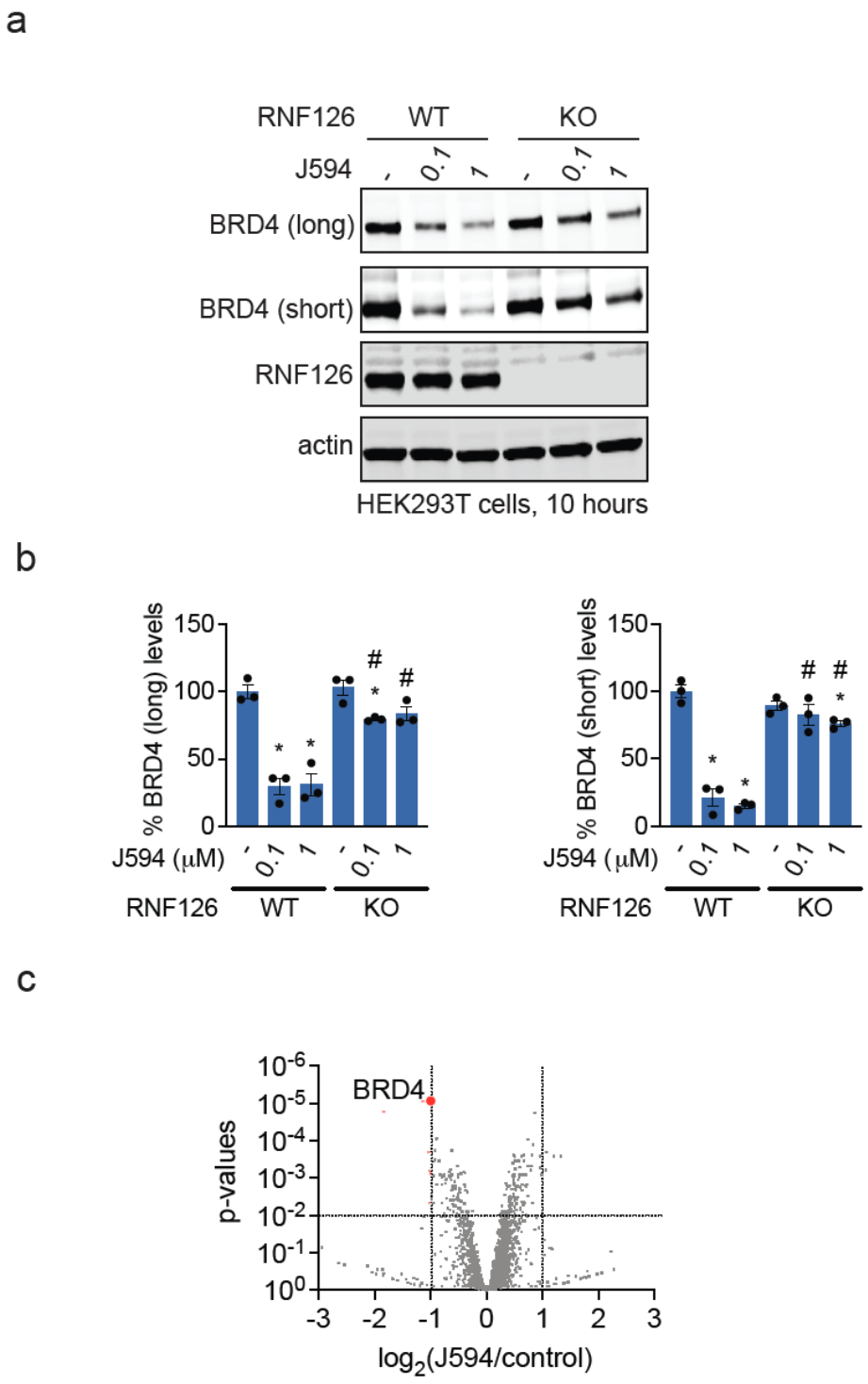

Figure 2.3 RNF126-dependent and selective BRD4 degradation by J594. (a) BRD4 degradation in RNF126 WT versus KO cells. RNF126 WT or KO HEK293T cells were treated with DMSO vehicle or J594 for 10 h, after which BRD4, RNF126, and loading control actin levels were assessed by SDS/PAGE and Western blotting. **(b)** Quantification

of BRD4 degradation in **(a)**. **(c)** Quantitative proteomic profiling of J594 in MBA-MB-231 cells. MDA-MB-231 cells were treated with DMSO vehicle or J594 (1 μM) for 24 h, after which proteomes were analyzed by tandem mass tagging (TMT)-based quantitative proteomics by LC-MS/MS. Blot in **(a)** is representative of n=3 biologically independent replicates per group. Bar graphs in **(b)** show individual replicates and average ± sem. Proteomic data is from n=3 biologically independent replicates per group, and the full dataset can be found in **Table S1.** Significance in **(b)** is expressed as *p<0.05 compared to vehicle-treated WT control and #p<0.05 compared to respective concentrations of WT conditions.

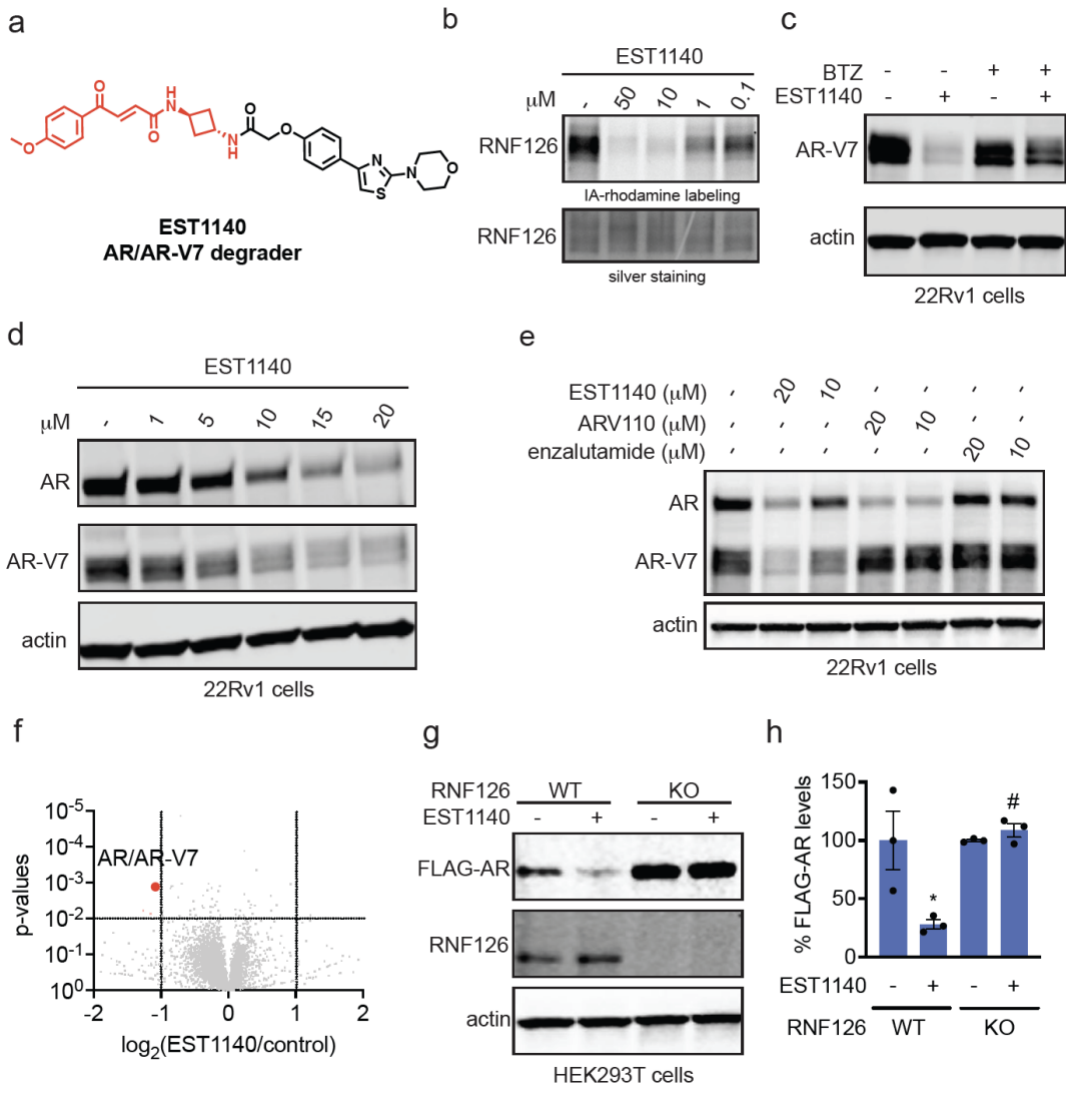

Figure 2.4 Transplantation of the optimized RNF126 handle enables AR and AR-V7 degradation. (a) Chemical structure of EST1140. **(b)** Gel-based ABPP of EST1140. RNF126 pure protein was pre-incubated with DMSO vehicle or EST1140 for 30 min prior to incubation with IA-rhodamine (100 nM) for 1 h, after which proteins were separated by SDS/PAGE and visualized by in-gel fluorescence. Loading was assessed by silver staining. **(c)** Proteasome-dependence of AR-V7 degradation. 22Rv1 cells were pre-treated with DMSO vehicle or proteasome inhibitor bortezomib for 1 h prior to treatment of cells with DMSO vehicle or EST1140 (20 μM) for 24 h, after which AR-V7 and loading control actin levels were assessed by SDS/PAGE and Western blotting. **(d,e)** Dose-response of EST1140, ARV110, and enzalutamide. 22Rv1 cells were treated with DMSO vehicle, EST1140, ARV110, or enzalutamide for 24 h, after which AR, AR-V7, and loading control actin levels were assessed by SDS/PAGE and Western blotting. **(f)** Quantitative proteomic profiling of EST1140 in 22Rv1 cells. 22Rv1 cells were treated with DMSO vehicle or EST1140 (20 μM) for 24 h, after which proteomes

were analyzed using TMT-based quantitative proteomics by LC-MS/MS. **(g)** AR degradation. FLAG-AR-expressing RNF126 WT versus KO HEK293T cells were treated with DMSO vehicle or EST1140 (20 μM) for 24 h, after which FLAG-AR, RNF126, and loading control actin levels were assessed by SDS/PAGE and Western blotting. **(h)** Quantification of the experiment described in **(h)**. Blots in **(b-e, g)** are representative of n=3 biologically independent replicates per group. Proteomic data in **(f)** is from n=3 biologically independent replicates per group, and the full dataset can be found in **Table S2.** Bar graph in **(h)** shows individual replicates and average ± sem. Significance in **(h)** is expressed as *p<0.05 compared to vehicle-treated WT control and #p<0.05 compared to EST1140-treated WT groups.

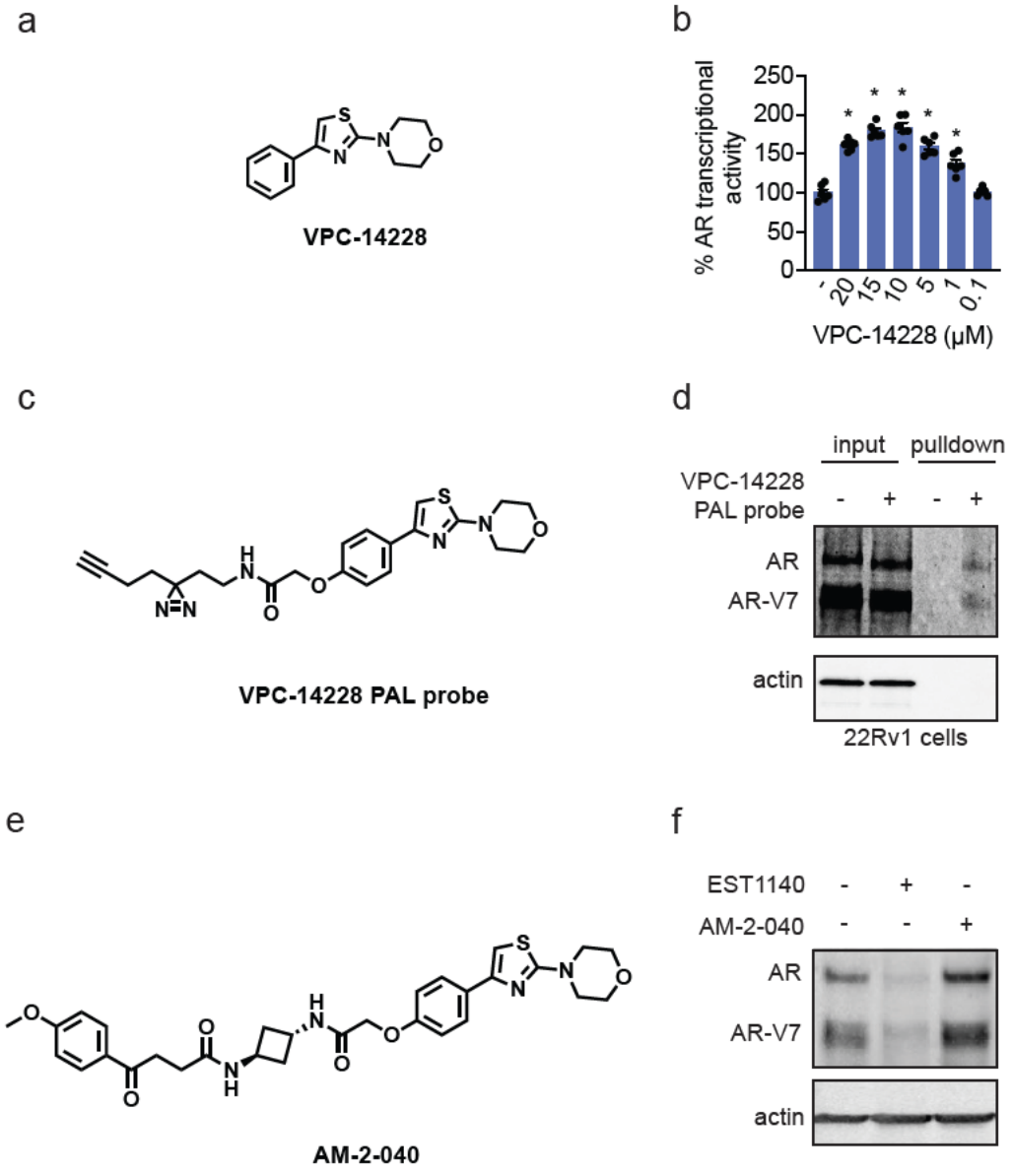

Figure 2.5 Characterization of VPC-14228 and non-reactive analogs of EST1140. **(a)** Structure of VPC-14228. **(b)** AR transcriptional activity in 22Rv1 cells. 22Rv1 cells expressing an AR luciferase reporter were treated with DMSO vehicle or VPC-14228 for 12 h, and total AR/AR-V7 transcriptional activity was assessed by luminescence. **(c)** Structure of alkyne-functionalized photoaffinity (PAL) probe based on VPC-14228. **(d)** Photoaffinity pulldown of AR and AR-V7. 22Rv1 cells were treated with DMSO vehicle or VPC-14228 PAL probe (20 μM) for 1h, after which cells were irradiated with hν for 30 min. Proteomes were subjected to copper-catalyzed alkyne-azide cycloaddition (CuAAC) with a biotin-functionalized azide enrichment handle, probe-labeled proteins were avidin-enriched, and eluted. Input proteome and pulldown proteins were separated by SDS/PAGE, and AR, AR-V7, and unrelated negative control protein actin were visualized by Western blotting. **(e)** Structure of unreactive analog of EST1140, AM-2-

040. **(f)** Comparing AR and AR-V7 degradation with EST1140 and AM-2-040. 22Rv1 cells were treated with DMSO vehicle, EST1140 (20 mM), or AM-2-040 (20 mM) for 24 h, after which AR, AR-V7, and loading control actin levels were assessed by SDS/PAGE and Western blotting. Bar graph in **(b)** show individual replicates and average ± sem from n=5 biologically independent replicates per group. Blots in **(d,f)** are representative of n=3 biologically independent replicates per group. Significance in **(b)** shown as *p<0.05 compared to vehicle-treated controls.

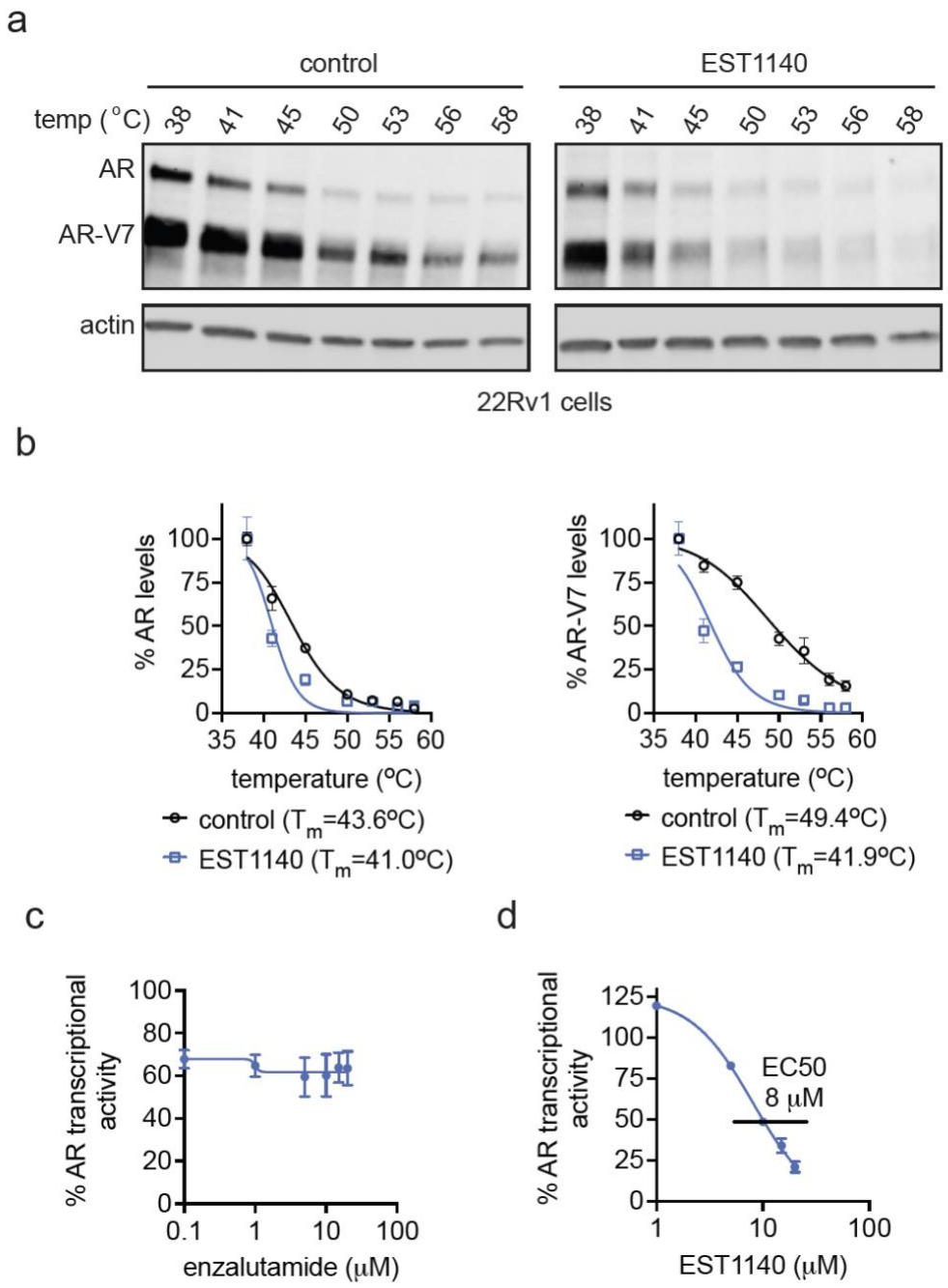

Figure 2.6 Functional consequences of AR/AR-V7 degradation by EST1140. (a) CETSA analysis demonstrating destabilization of AR and AR-V7. 22Rv1 cells were treated with DMSO vehicle or EST1140 (10 mM) for 1 h, after which cells were heated to designated temperatures, precipitated proteins were cleared, and AR, AR-V7, and actin control levels were assessed by SDS/PAGE and Western blotting. **(b)** Quantification of CETSA data in **(a). (c,d)** Inhibition of AR transcriptional activity by EST1140. 22Rv1 cells expressing an AR luciferase reporter were treated with DMSO vehicle, enzalutamide **(c)**, or EST1140 **(d)** for 12 h, and total AR/AR-V7 transcriptional

activity was assessed by luminescence. Blot in **(a)** is representative of n=3 biologically independent replicates per group. Graphs in **(b-d)** show average ± sem values of n=3 biologically independent replicates per group.

2.5 Methods

2.5.1 Cell Culture

HEK293T and MDA-MB-231 cells were purchased from the UC Berkeley Cell Culture Facility and were cultured in DMEM containing 10% (v/v) FBS. 22Rv1 cells were purchased from the UC Berkeley Cell Culture Facility and were cultured in RPMI 1640 containing 10% (v/v) FBS. AIZ-AR stable 22Rv1 luciferase reporter cells were purchased from Applied Biological Materials (T3104) and were cultured in RPMI 1640. All cell lines were maintained at 37°C with 5% CO_2.

2.5.2 Expression and purification of recombinant RNF126 protein

RNF126 mammalian expression plasmid with a C-terminal FLAG tag was purchased from Origene (Origene Technologies Inc., RC204986). The plasmid was transformed into NEB 5-alpha Competent E. coli (DH5a) cells (NEB product no. C2987H). The following day, a single transformed colony was used to inoculate 50 mL of nutrient rich LB medium containing kanamycin (50 µg/mL) and was incubated at 37 ^{o}C overnight, with agitation (250 rpm). A Miniprep (Qiagen) kit was used to isolate the plasmid before sequence verification with appropriate primers. HEK293T cells were grown to 30-50% confluency in DMEM supplemented with 10% FBS (Corning) and maintained at 37°C with 5% CO2. Immediately before transfection, media was replaced with DMEM containing 10% FBS. Each plate was transfected with 24 µg of overexpression plasmid with 24 µL Lipofectamine 2000 (Invitrogen) in Opti-MEM. After 48 h cells were collected in PBS, lysed by sonication, and batch bound with anti-DYKDDDDK resin (GenScript, L00432) for 2 hours. Lysate and resin were washed with PBS and eluted with 133.33 µg/mL 3X FLAG peptide (ApexBio, A6001) in PBS. Five elutions were performed for 15 minutes each. Elutions were concentrated and the protein was stored in PBS. Concentration and purity were determined using the BCA assay and Western blotting.

2.5.3 Cell Lysate Preparation

Cells were washed with PBS, harvested by scraping, and pelleted by centrifugation (1400*g*, 4 min, 4 °C). Pellets were resuspended in PBS, and lysed by sonication or RIPA lysis buffer (supplemented with Pierce protease inhibitor mini tablets, EDTA-free, Thermo Fisher Scientific, A32955). Unless otherwise stated, total lysate was utilized for Western blotting and chemoproteomics experiments. Protein concentrations were determined using the BCA assay (Pierce, 23225). Lysates were stored at −80°C, or taken for Western blotting or chemoproteomics experiments.

2.5.4 Western Blotting

Anti-GAPDH (Cell Signaling Technology, D4C6R), β-actin (Cell Signaling Technology, E4D9Z), BRD4 (Abcam ab128874), AR (Cell Signaling Technology, D6F11), RNF126 (Santa Cruz Biotechnology sc-376005), were obtained, and dilutions were prepared in accordance with the manufacturer's recommended protocol. Proteins were resolved by SDS/PAGE and transferred to nitrocellulose membranes using the Trans-Blot Turbo transfer system (Bio-Rad). Membranes were blocked with 5% BSA in Tris-buffered saline containing Tween 20 (TBS-T) solution for 1 hr at RT washed in TBS-T, and probed with primary antibody diluted in recommended diluent per manufacturer overnight at 4 °C. After 3 washes with TBS-T, the membranes were incubated in the dark with IR680- or IR800-conjugated secondary antibodies at 1:10,000 dilution in 5 % BSA in TBS-T at RT for
1 h. After 3 additional washes with TBST, blots were visualized using an Odyssey Li-Cor fluorescent scanner. The membranes were stripped using ReBlot Plus Strong Antibody Stripping Solution (EMD Millipore, 2504) when additional primary antibody incubations were performed.

2.5.5 Knockdown Studies

Short-hairpin oligonucleotides were used to knock down the expression of RNF126 in HEK293T cells. For lentivirus production, lentiviral plasmids and packaging plasmids (pMD2.G, Addgene catalog no. 12259 and psPAX2, Addgene catalog no. 12260) were transfected into HEK293T cells using Lipofectamine 2000 (Invitrogen). Lentivirus was collected from filtered cultured medium and used to infect the target cell line with 1:1000 dilution of polybrene. Target cells were selected over 3 days with 1 μg/mL of puromycin for HEK293T cells. The short-hairpin sequences which were used for generation of the knockdown lines were: RNF126: TGCCATCATCACACAGCTCCT (Sigma RNF126 MISSION shRNA Bacterial Glycerol Stock, TRCN0000368954). MISSION TRC1.5 pLKO.1- or TRC2 pLKO.5-puro Non-Mammalian shRNA Control (Sigma) was used as a control shRNA.

2.5.6 Gel Based ABPP

Recombinant RNF126 (0.1μg/sample) was pre-treated with either DMSO vehicle or covalent ligand at 37 °C for 30 min in 25 μL of PBS and subsequently treated with IA-Rhodamine (concentrations designated in figure legends) (Setareh Biotech) at room temperature for 1 h in the dark. The reaction was stopped by addition of 4x reducing Laemmli SDS sample loading buffer (Alfa Aesar). After boiling at 95 °C for 5 min, the samples were separated on precast 4−20% Criterion TGX gels (Bio-Rad). Probe-labeled proteins were analyzed by in-gel fluorescence using a ChemiDoc MP (Bio-Rad).

2.5.7 Quantitative TMT Proteomics Analysis

Cells were treated with DMSO vehicle or compound for 24 h and lysates were prepared as described above. 25-100ug of lysate was reduced, alkylated and digested with sequencing grade trypsin overnight. Individual samples were then labeled with isobaric tags using commercially available TMTsixplex (Thermo Fisher Scientific, P/N 90061) kits, in accordance with the manufacturer's protocols. Tagged samples (20 µg per sample) were combined, dried using a vacuum concentrator at 30 °C, resuspended with 300 µL 0.1% TFA in H_2O, and fractionated using high pH reversed-phase peptide fractionation kits (Thermo Fisher Scientific, P/N 84868) according to the manufacturer's protocol. Fractions were dried using a vacuum concentrator at 30 °C, resuspended with 50 µL 0.1% FA in H_2O, and analyzed by LC-MS/MS as described below.

Quantitative TMT-based proteomic analysis was performed as previously described using a Thermo Eclipse with FAIMS LC-MS/MS. Acquired MS data was processed using ProLuCID (in IP2 v.3-v.5, (Integrated Proteomics Applications, Inc.)) or SagePro (in Chaparral Laboratories, Inc.). Trypsin cleavage specificity (cleavage at K, R except if followed by P) allowed for up to 2 missed cleavages. Carbamidomethylation of cysteine was set as a fixed modification, methionine oxidation and TMT-modification of N-termini and lysine residues were set as variable modifications. Reporter ion ratio calculations were performed using summed abundances with most confident centroid selected from a 20 ppm window. Only peptide-to-spectrum matches that are unique assignments to a given identified protein within the total dataset are considered for protein quantitation. High confidence protein identifications were reported with a <1% false discovery rate (FDR) cut-off. Differential abundance significance was estimated using ANOVA with Benjamini-Hochberg correction to determine p-values.

2.5.8 AM-2-012 Pure Protein Competitive Click Pulldown

0.5 µg of RNF126 recombinant protein was treated with DMSO vehicle or 50µM EST1140 in 50 µL PBS for 30 min at 37°C. Samples were subsequently treated with DMSO vehicle or AM-2-012 for 30 min at RT. CuAAC) was performed by addition of 0.25 µL Azide-Fluor 545 (5mM in DMSO, Click Chemistry Tools, Inc. product #AZ109-5), 1 µL $CuSO_4$ (50mM in H_2O), 3 µL TBTA (0.9 mg/mL in 4:1 tBuOH/DMSO) and 1 µL TCEP (14.4 mg/mL in H_2O). After one hour at RT, 30 µL 4x Laemlli's buffer was added. Probe-labeled proteins were analyzed by in-gel fluorescence using a ChemiDoc MP (Bio-Rad).

2.5.9 Cellular Thermal Shift Assay (CETSA)

22Rv1 cells were harvested by scraping from a 10 cm dish after 1 hour at 50 µM compound treatment. Cells were resuspended in PBS containing protease inhibitor cocktail and 50 µM compound and then aliquoted into eight 0.2 mL PCR strips with 100

µL per tube. PCR strips were designated a temperature via a gradient program on Bio-Rad's T100 Thermal cycler (Bio-Rad, 1861096). Samples were heated at their respective temperatures (37°C, 38°C, 41°C, 45°C, 50°C, 53°C, 56°C, 58°C) for 3 minutes and then at 25 °C for 3 minutes. Immediately following, cells were snap-lysed using liquid nitrogen (3 freeze-thaw cycles). Cell debris, along with any precipitated and aggregated proteins, were removed by centrifugation at 20,000 g for 20 minutes at 4 °C. 80 µL of supernatant was transferred to new PCR strips, 26.6 µL of 4x reducing Laemmli SDS sample loading buffer was added to each sample and boiled at 95°C for 10 minutes. Probe-labeled proteins were analyzed by in-gel fluorescence using an Odyssey DLx Imager (LICORbio).

III. CONCLUDING REMARKS

The work described in this dissertation addresses a central challenge in the field of targeted protein degradation: the rational, chemistry-centric design of molecular glue degraders with translational potential. By developing an optimized RNF126-targeting covalent handle that overcomes the reactivity and cytotoxicity limitations of the first-generation fumarate scaffold, we have established a practical and modular platform for molecular glue degrader development.

Our findings demonstrate several key principles. First, the electrophilic handle in a covalent molecular glue degrader is not a fixed structural element but rather an independently optimizable chemical module. The transition from a fumarate-based electrophile to a *trans*-cyclobutane linker preserved RNF126 engagement while markedly improving glutathione stability and reducing cellular toxicity. This principle that handle optimization can decouple reactivity from degradative function should broadly inform future molecular glue degrader campaigns.

Second, the modularity and transplantability of the optimized handle were validated across structurally and biologically distinct target contexts. The successful degradation of BRD4 confirmed that the optimized handle retains the core attributes of the original scaffold, while the extension to AR and AR-V7 demonstrated its applicability to clinically relevant, undruggable targets. The ability of EST1140 to degrade both AR and AR-V7—and to suppress AR-dependent transcriptional activity more effectively than enzalutamide—highlights the therapeutic potential of RNF126-based molecular glue degradation in androgen-independent prostate cancer.

Third, these results contribute to a broader understanding of the covalent molecular glue degrader landscape. Together with parallel efforts targeting DCAF16, DCAF11, FBXO22, RNF4, RNF114, and FEM1B,[5–9,18–26] our work underscores that covalent engagement of E3 ligase cysteines is a powerful and generalizable strategy for enabling degradation. The emerging diversity of druggable E3 ligases and cysteine sites suggests that the chemical space available for covalent molecular glue degrader design is far larger than currently exploited.

Looking forward, several important directions remain. The in vivo pharmacology of optimized RNF126-targeting handles warrants thorough investigation, including pharmacokinetic profiling, tolerability studies, and efficacy evaluation in preclinical prostate cancer models. Further handle optimization, through systematic variation of electrophile geometry, linker length, and stereochemistry, may yield next-generation scaffolds with enhanced potency and selectivity profiles. Additionally, expanding the target scope to other transcription factors and intrinsically disordered proteins will test the generalizability and limits of this platform. Extending the covalent handle to heterobifunctional contexts may increase the utility of the fumarate warhead towards targets that may not be degradable through a molecular glue-type mechanism.

An additional next step may consist of synthesizing libraries of RNF126-warhead derived compounds and evaluating the substrate space that is degradable by this E3 ligase. Similar studies have been undertaken with CRBN, where a beta-hairpin (‘G-loop’) was identified as a key recognition motif. Targets bearing this secondary structure, such as VAV1 and GSPT1, were able to be degraded despite a lack of ligandable binding pocket. Similar targets amenable to RNF126-mediated degradation could be identified, providing an additional path to address the undruggable proteome. In conclusion, this dissertation establishes an optimized chemical blueprint for RNF126-based molecular glue degraders and demonstrates their utility against both classically druggable and undruggable protein targets. By treating the covalent handle as an optimizable module within a rational design framework, we provide a foundation for the continued development of molecular glue degraders as a therapeutic modality.

References

1. De La Torre, B. G. & Albericio, F. The Pharmaceutical Industry in 2025: An Analysis of FDA Drug Approvals from the Perspective of Molecules. *Molecules* **31**, 419 (2026).
2. Strelow, J. M. A Perspective on the Kinetics of Covalent and Irreversible Inhibition. *SLAS Discov.* **22**, 3–20 (2017).
3. Hong, D. S. *et al.* $KRAS^{G12C}$ Inhibition with Sotorasib in Advanced Solid Tumors. *N. Engl. J. Med.* **383**, 1207–1217 (2020).
4. Huang, F., Han, X., Xiao, X. & Zhou, J. Covalent Warheads Targeting Cysteine Residue: The Promising Approach in Drug Development. *Molecules* **27**, 7728 (2022).
5. Bond, M. J. & Crews, C. M. Proteolysis targeting chimeras (PROTACs) come of age: entering the third decade of targeted protein degradation. *RSC Chem. Biol.* **2**, 725–742 (2021).
6. Salvaris, R. T., Brennan, J. & Lewis, K. L. BTK Is the Target That Keeps on Giving: A Review of BTK-Degrader Drug Development, Clinical Data, and Future Directions in CLL. *Cancers* **17**, 557 (2025).
7. Nunes, J. *et al.* Targeting IRAK4 for Degradation with PROTACs. *ACS Med. Chem. Lett.* **10**, 1081–1085 (2019).
8. Xiang, W. *et al.* Discovery of ARD-1676 as a Highly Potent and Orally Efficacious AR PROTAC Degrader with a Broad Activity against AR Mutants for the Treatment of AR + Human Prostate Cancer. *J. Med. Chem.* **66**, 13280–13303 (2023).
9. Zammit, C. M. *et al.* Covalent Destabilizing Degrader of AR and AR-V7 in Androgen-Independent Prostate Cancer Cells. *J. Am. Chem. Soc.* **147**, 20512–20524 (2025).
10. King, E. A., Meyers, M. & Nomura, D. K. Induced proximity-based therapeutic modalities. *Nat. Rev. Drug Discov.* **25**, 175–203 (2026).

11. Rehman, W., Arfons, L. M. & Lazarus, H. M. The rise, fall and subsequent triumph of thalidomide: lessons learned in drug development. *Ther. Adv. Hematol.* **2**, 291–308 (2011).

12. Krönke, J. *et al.* Lenalidomide induces ubiquitination and degradation of CK1α in del(5q) MDS. *Nature* **523**, 183–188 (2015).

13. Petzold, G., Fischer, E. S. & Thomä, N. H. Structural basis of lenalidomide-induced CK1α degradation by the CRL4CRBN ubiquitin ligase. *Nature* **532**, 127–130 (2016).

14. Petzold, G. *et al.* Mining the CRBN target space redefines rules for molecular glue–induced neosubstrate recognition. *Science* **389**, eadt6736 (2025).

15. Toriki, E. S. *et al.* Rational Chemical Design of Molecular Glue Degraders. *ACS Cent. Sci.* **9**, 915–926 (2023).

16. Orr, L. M. *et al.* DCAF16-Based Covalent Degradative Handles for the Modular Design of Degraders. *ACS Cent. Sci.* **11**, 1207–1217 (2025).

17. Lim, M. *et al.* DCAF16-Based Covalent Handle for the Rational Design of Monovalent Degraders. *ACS Cent. Sci.* **10**, 1318–1331 (2024).

18. Hassan, M. M. *et al.* Exploration of the tunability of BRD4 degradation by DCAF16 trans-labelling covalent glues. *Eur. J. Med. Chem.* **279**, 116904 (2024).

19. Li, Y.-D. *et al.* Template-assisted covalent modification underlies activity of covalent molecular glues. *Nat. Chem. Biol.* **20**, 1640–1649 (2024).

20. Basu, A. A. *et al.* A CRISPR activation screen identifies FBXO22 supporting targeted protein degradation. *Nat. Chem. Biol.* **20**, 1608–1616 (2024).

21. Sarott, R. C. *et al.* Chemical Specification of E3 Ubiquitin Ligase Engagement by Cysteine-Reactive Chemistry. *J. Am. Chem. Soc.* **145**, 21937–21944 (2023).

22. Ward, C. C. *et al.* Covalent Ligand Screening Uncovers a RNF4 E3 Ligase Recruiter for Targeted Protein Degradation Applications. *ACS Chem. Biol.* **14**, 2430–2440 (2019).

23. Zhang, X., Crowley, V. M., Wucherpfennig, T. G., Dix, M. M. & Cravatt, B. F. Electrophilic PROTACs that degrade nuclear proteins by engaging DCAF16. *Nat. Chem. Biol.* **15**, 737–746 (2019).

24. Spradlin, J. N. *et al.* Harnessing the anti-cancer natural product nimbolide for targeted protein degradation. *Nat. Chem. Biol.* **15**, 747–755 (2019).

25. Neklesa, T. K. *et al.* Small-molecule hydrophobic tagging–induced degradation of HaloTag fusion proteins. *Nat. Chem. Biol.* **7**, 538–543 (2011).

26. Molina, D. M. *et al.* Monitoring Drug Target Engagement in Cells and Tissues Using the Cellular Thermal Shift Assay. *Science* **341**, 84–87 (2013).

27. Gowans, F. A. *et al.* Covalent Degrader of the Oncogenic Transcription Factor β-Catenin. *J. Am. Chem. Soc.* **146**, 16856–16865 (2024).

28. Do, T. C. *et al.* Covalent Modulators of Immune Regulatory Transcription Factors IRF8 and IRF5. Preprint at https://doi.org/10.1101/2025.08.03.668300 (2025).

29. Modi, A. *et al.* An Optimized RNF126-Targeting Covalent Handle for Molecular Glue Degraders. Preprint at https://doi.org/10.64898/2026.03.06.709959 (2026).

30. Sobhani, N. *et al.* AR-V7 in Metastatic Prostate Cancer: A Strategy beyond Redemption. *Int. J. Mol. Sci.* **22**, 5515 (2021).

31. Uo, T., Plymate, S. R. & Sprenger, C. C. The potential of AR-V7 as a therapeutic target. *Expert Opin. Ther. Targets* **22**, 201–216 (2018).

32. Scott, L. J. Enzalutamide: A Review in Castration-Resistant Prostate Cancer. *Drugs* **78**, 1913–1924 (2018).

33. Neklesa, T. *et al.* ARV-110: An oral androgen receptor PROTAC degrader for prostate cancer. *J. Clin. Oncol.* **37**, 259–259 (2019).

34. Bhumireddy, A. *et al.* Design, synthesis, and biological evaluation of phenyl thiazole-based AR-V7 degraders. *Bioorg. Med. Chem. Lett.* **55**, 128448 (2022).

35. Dalal, K. *et al.* Selectively Targeting the DNA-binding Domain of the Androgen Receptor as a Prospective Therapy for Prostate Cancer. *J. Biol. Chem.* **289**, 26417–26429 (2014).

36. Axelsson, H., Almqvist, H., Seashore-Ludlow, B. & Lundbäck, T. Screening for Target Engagement using the Cellular Thermal Shift Assay - CETSA. in *Assay Guidance Manual* (eds Sittampalam, G. S. et al.) (Eli Lilly & Company and the National Center for Advancing Translational Sciences, Bethesda (MD), 2004).

37. Zammit, C. M. *et al.* Covalent Destabilizing Degrader of AR and AR-V7 in Androgen-Independent Prostate Cancer Cells. *J. Am. Chem. Soc.* **147**, 20512–20524 (2025).

APPENDICES

Supplementary Figures

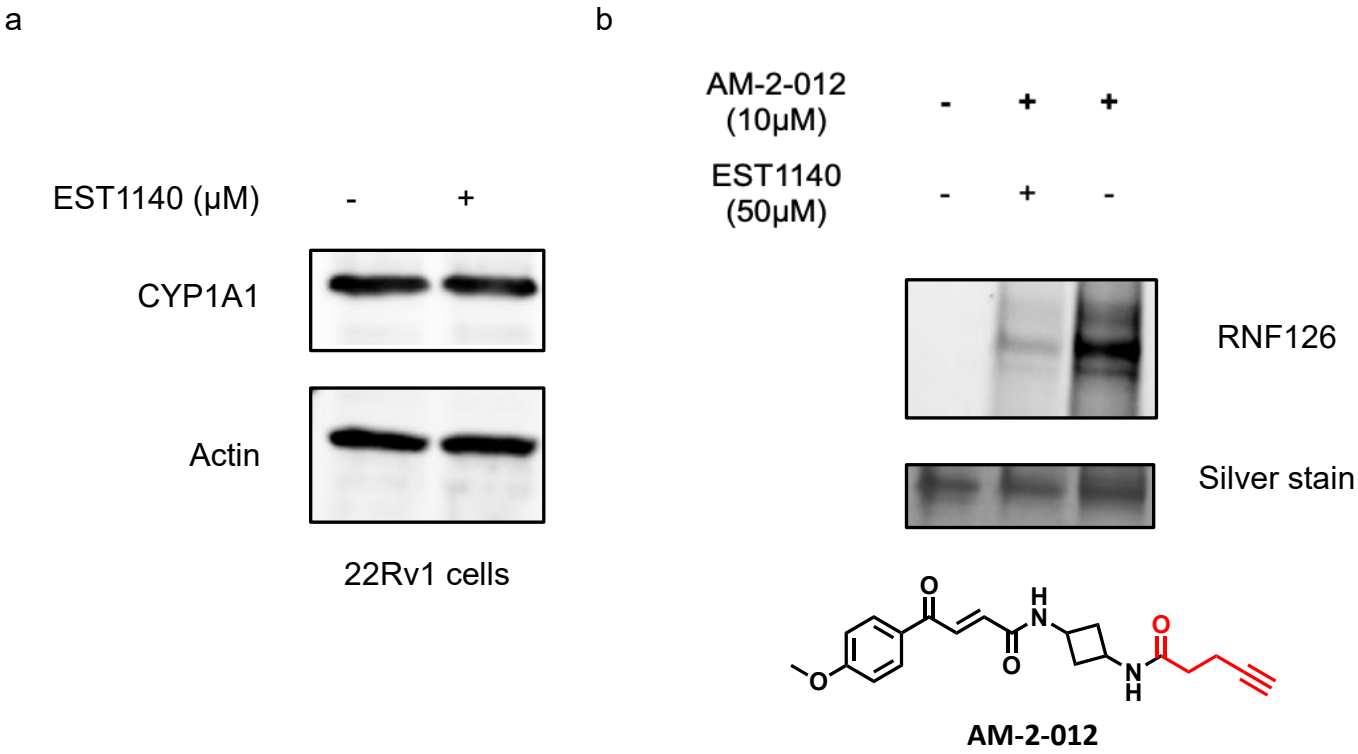

Supplementary Figure S1 a) EST1140 does not lead to loss of CYP1A1, one of the major downregulated proteins detected via TMT proteomics. b) An RNF126-directed alkyne probe labels recombinant RNF126 upon CuAAC reaction with rhodamine-azide, and signal is outcompeted by pretreatment of EST1140.

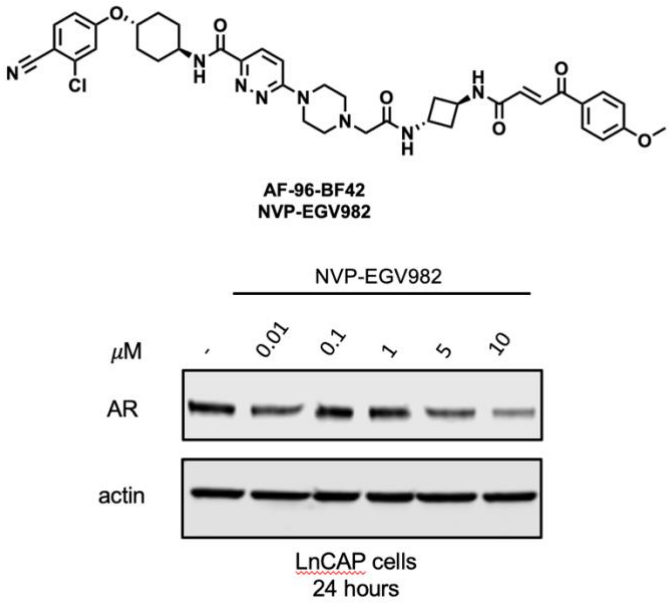

Supplementary Figure S2 NVP-EGV982 degrades full-length AR in androgen-sensitive LnCAP cells.

Synthetic Methods and Characterization

Amide Couplings

General Procedure A

A mixture of the carboxylic acid (1.1 equiv.) and HATU (2 equiv.) was purged with N_2 for 5 minutes. The mixture was dissolved in *N,N*-dimethylformamide (0.1M). *N,N*-diisopropylethylamine (DIPEA, 3 equiv.) was transferred to the reaction mixture. The reaction was stirred at ambient temperature for 15 minutes. The amine was purged with N_2 in a separate vial, dissolved in a minimal amount of DMF and transferred to the reaction. The reaction mixture was stirred at ambient temperature overnight. The reaction was quenched with 5X volume of 5% LiCl (aq.) and extracted thrice with ethyl acetate (EtOAc) or dichloromethane (DCM). Organic layers were dried over Na_2SO_4, filtered and concentrated *in vacuo*. Crude reactions were purified by silica gel flash chromatography to yield the title compound.

General Procedure B

The carboxylic acid (1.1 equiv.) was purged with N_2 for 5 minutes and dissolved in DMF (0.1M). DIPEA (3 equiv.) to which propylphosphonic anhydride solution (>50 wt.% in EtOAc, 1.1 equiv.) was transferred. The reaction mixture was stirred at ambient temperature for 30 minutes. The amine was purged with N_2 in a separate vial, dissolved in a minimal amount of DMF and transferred. The reaction was stirred at ambient temperature overnight. The reaction was quenched with 5X volume of 5% LiCl (aq) and extracted thrice with ethyl acetate (EtOAc) or dichloromethane (DCM). Organic layers were dried over Na_2SO_4, filtered and concentrated *in vacuo*. Crude reactions were purified by silica gel flash chromatography to yield the title compound.

General Procedure C

The corresponding tert-butyloxycarbonyl protected amine was dissolved in a 1:1 mixture of DCM:Trifluoroacetic acid (30 equiv.). The reaction mixture was stirred for 30 min – 1 hour. The volatiles were removed *in vacuo* and crude residue was used without further purification.

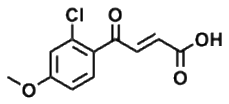

Acid-059

To a solution of 3-chloroanisole (1.5 g, 15.30 mmol) and maleic anhydride (2.0 g, 13.91 mmol) in DCM (50 mL) was added $AlCl_3$ (3.7 g, 27.81 mmol) portion wise. The mixture was stirred at room temperature for 24 hrs under N_2. The reaction mixture was quenched by ice-cooled 6N HCl (300 mL) and extracted with DCM (100 mL). The organic layer was washed with saturated $NaHCO_3$ aq. (300 mL). The water layer was adjusted to pH=3 with 1N HCl and extracted with DCM (100 mL x3). The combined organic layers were washed with brine (200 mL), dried over Na_2SO_4, filtered and concentrated to give crude product. The crude was purified by silical gel chromatography (EtOAc:Petroleum ether = 0 – 100%) to give Acid- 059 (1.4 g, 5.82 mmol, 41.8%) as a yellow solid.

^{1}H NMR (500 MHz, DMSO) δ 7.72 (d, *J* = 8.7 Hz, 1H), 7.38 (d, *J* = 15.7 Hz, 1H), 7.23 (d, *J* = 2.5 Hz, 1H), 7.11 (dd, *J* = 8.7, 2.5 Hz, 1H), 6.54 (d, *J* = 15.7 Hz, 1H), 3.92 (s, 3H).

^{13}C NMR (126 MHz, DMSO) δ 197.16, 191.43, 173.33, 167.05, 163.70, 162.72, 162.55, 138.03, 133.48, 133.06, 132.83, 132.66, 129.70, 128.33, 116.56, 116.33, 113.84, 113.40, 56.50, 56.39, 41.04, 40.57, 40.48, 40.40, 40.31, 40.23, 40.14, 40.07, 39.98, 39.90, 39.81, 39.64, 39.48.

HRMS (ESI): m/z calculated for $[C_{11}H_9ClO_4 + Na]^+$ = 263.0082, found 263.0088

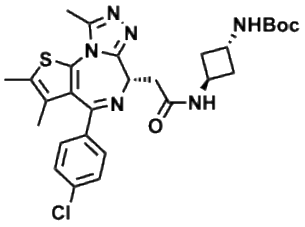

JQ1_PASW

Synthesized using General Procedure A, with (+)-JQ1-acid (100 mg, 0.25 mmol), tert-Butyl (trans-3-aminocyclobutyl)carbamate (022 mmol, 41.82 mg), HATU (142.3 mg, 0.374 mmol) and DIPEA (0.133 mL, 0.748 mmol). The crude residue was purified by silica gel chromatography (0 – 10% MeOH in DCM
) to afford 74 mg of the title compound (52.1%) as a brown solid.

^{1}H NMR (500 MHz, $CDCl_3$) δ 7.36 – 7.30 (m, 2H), 7.28 – 7.24 (m, 2H), 4.78 – 4.68 (m, 1H), 4.54 (dd, *J* = 7.6, 6.4 Hz, 1H), 4.37 (p, *J* = 7.2 Hz, 1H), 4.14 (s, 1H), 3.47 (dd, *J* = 14.3, 7.6 Hz, 1H), 3.32 – 3.21 (m, 1H), 2.60 (s, 3H), 2.36 – 2.29 (m, 4H), 2.28 – 2.23 (m, 2H), 2.19 (ddd, *J* = 12.7, 6.5, 3.6 Hz, 1H), 1.60 (s, 3H), 1.37 (s, 9H).

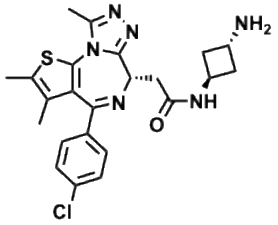

JQ1_PASW-NH_2

To a solution of **JQ1_PASW** (200 mg, 0.35 mmol, 1.0 eq.) in HCl/EtOAc (5 mL) and stirred at 25°C for 1 hr under N_2. The reaction mixture was concentrated under reduced pressure to give the title compound (200 mg, crude) as a yellow oil.

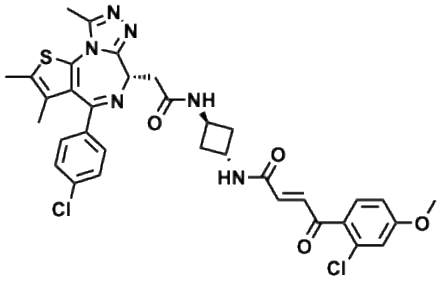

NVP-IKJ594

To a solution of **Acid-059** (74 mg, 0.30 mmol, 1.2 eq.), compound **JQ1_PASW-NH_2** (120 mg, 0.25 mmol, 1.0 eq.) and BOP (124 mg, 0.28, 1.1 eq.) in DMF (2 mL) was added DIPEA (0.221 mL, 1.28 mmol, 5.0 eq.). The mixture was stirred at room temperature overnight under N_2. The reaction mixture was quenched by 1N HCl (10

mL) and extracted with EtOAc (10 mL x 3). The combined organic layers were washed by brine (50 mL), dried over Na_2SO_4, filtered and concentrated under reduced pressure to give the residue. The crude product was purified by column (EtOAc:Petroleum ether = 0 – 100%) to afford the title compound as an off-white solid.

^{1}H NMR (500 MHz, DMSO) δ 8.90 (dd, *J* = 11.5, 7.2 Hz, 1H), 8.60 (d, *J* = 7.0 Hz, 1H), 7.52 (dd, *J* = 48.3, 8.5 Hz, 1H), 7.43 (dd, *J* = 8.7, 1.7 Hz, 2H), 7.37 – 7.33 (m, 2H), 7.27 – 7.09 (m, 1H), 7.03 (dd, *J* = 8.4, 2.2 Hz, 1H), 6.77 – 6.64 (m, 1H), 4.43 (dd, *J* = 8.2, 6.1 Hz, 1H), 4.35 (hept, *J* = 6.5 Hz, 1H), 4.24 (h, *J* = 6.6 Hz, 1H), 3.81 (d, *J* = 15.6 Hz, 3H), 3.26 – 3.08 (m, 2H), 2.53 (s, 3H), 2.34 (s, 3H), 1.55 (s, 3H).

13C NMR (126 MHz, DMSO) δ 191.84, 169.68, 163.58, 155.54, 150.39, 137.20, 136.21, 135.73, 135.67, 132.73, 132.39, 131.26, 130.60, 130.32, 130.03, 128.99, 121.30, 116.24, 113.82, 72.94, 63.54, 57.01, 56.49, 54.33, 41.93, 41.50, 40.43, 40.35, 40.26, 40.18, 40.09, 40.02, 39.93, 39.76, 39.59, 39.43, 38.02, 36.90, 14.52, 13.14, 11.76.

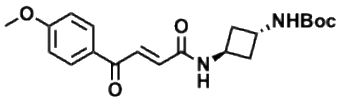

EST1127

Synthesized using General Procedure A, with (*E*)-4-(4-methoxyphenyl)-4-oxobut-2-enoic acid (0.890 g, 4.32 mmol), tert-Butyl (trans-3-aminocyclobutyl)carbamate (803.9 mg, 4.32 mmol), HATU (2.75 g, 8.63 mmol) and DIPEA (2.31 mL, 12.95 mmol). The crude residue was purified by silica gel chromatography (0 – 15% MeOH in DCM) to afford 312 mg of the title compound (19.3%) as a brown solid.

^{1}H NMR (500 MHz, $CDCl_3$) δ 8.08 – 8.01 (m, 2H), 7.94 (d, *J* = 15.1 Hz, 1H), 7.02 – 6.94 (m, 3H), 4.50 – 4.41 (m, 1H), 4.24 – 4.18 (m, 1H), 3.90 (s, 3H), 2.59 (s, 2H), 2.35 (h, *J* = 5.9 Hz, 4H), 1.44 (s, 9H).

^{13}C NMR (126 MHz, $CDCl_3$) δ 188.59, 164.51, 164.35, 155.74, 134.88, 134.83, 132.93, 131.47, 129.95, 114.20, 79.81, 77.40, 77.15, 76.90, 55.63, 49.98, 49.81, 49.63, 49.46, 49.29, 49.12, 48.95, 42.85, 41.85, 37.48, 37.46, 28.39.

HRMS (ESI): m/z calculated for $[C_{20}H_{26}N_2O_5 + Na]^+$ = 397.1734, found 397.1725

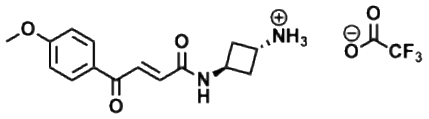

AM-2-011

Synthesized using General Procedure C.

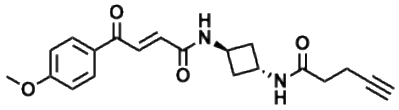

AM-2-012

Synthesized using General Procedure A, with **AM-2-011** (90 mg, 0.328 mmol), pent-4-ynoic acid (38.62 mg, 0.394 mmol), HATU (249.5 mg, 0.656 mmol), DIPEA (0.234 mL, 1.31 mmol). The crude residue was purified by silica gel chromatography (0-10% MeOH in DCM) to afford 42 mg of the title compound (36.12%) as a beige solid.

^{1}H NMR (500 MHz, DMSO) δ 8.93 (d, *J* = 7.2 Hz, 1H), 8.30 (d, *J* = 7.1 Hz, 1H), 8.04 – 7.96 (m, 2H), 7.75 (d, *J* = 15.3 Hz, 1H), 7.11 – 7.05 (m, 2H), 6.92 (d, *J* = 15.3 Hz, 1H), 4.35 (qd, *J* = 6.9, 1.1 Hz, 1H), 4.30 – 4.22 (m, 1H), 3.85 (s, 3H), 2.75 (t, *J* = 2.6 Hz, 1H), 2.37 – 2.30 (m, 2H), 2.27 – 2.18 (m, 6H).

^{13}C NMR (126 MHz, DMSO) δ 188.21, 170.25, 164.18, 163.47, 136.08, 132.28, 131.62, 129.99, 114.77, 84.21, 71.79, 56.14, 55.38, 41.82, 41.42, 40.57, 40.48, 40.41, 40.32, 40.24, 40.15, 40.07, 39.98, 39.81, 39.65, 39.48, 37.17, 34.59, 14.65.

HRMS (ESI): m/z calculated for $[C_{20}H_{22}N_2O_4 + H]^+$ = 355.1652, found 355.1644

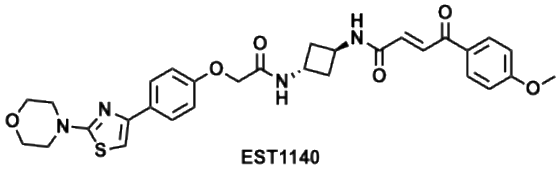

EST1140

Synthesized using General Procedure A, with **AM-2-011** (162.68 mg, 0.418 mmol), tert-butyl 2-(4-(2-morpholinothiazol-4-yl)phenoxy)acetate (122 mg, 0.381 mmol), HATU (289.6 mg, 0.761 mmol), DIPEA (0.339 mL, 1.90 mmol). The crude residue was purified by silica gel chromatography (0-10% MeOH in DCM) to afford 77.8 mg of the title compound (35.43%) as an off white solid.

^{1}H NMR (500 MHz, DMSO) δ 8.51 (d, *J* = 7.5 Hz, 1H), 8.35 (d, *J* = 7.1 Hz, 1H), 8.03 – 7.98 (m, 2H), 7.88 – 7.82 (m, 2H), 7.21 (s, 1H), 7.12 – 7.07 (m, 2H), 7.06 – 7.00 (m, 2H), 4.54 (s, 2H), 4.49 – 4.40 (m, 1H), 4.28 (tq, *J* = 7.6, 3.9 Hz, 1H), 3.90 (s, 3H), 3.82 – 3.76 (m, 4H), 3.49 (dd, *J* = 5.9, 3.8 Hz, 4H), 3.23 (t, *J* = 6.8 Hz, 2H), 2.49 (t, *J* = 6.7 Hz, 2H), 2.33 (ddd, *J* = 11.0, 8.2, 5.7 Hz, 2H), 2.23 (ddd, *J* = 12.5, 8.0, 5.0 Hz, 2H).

^{13}C NMR (101 MHz, DMSO-D_6) δ 188.29, 171.22, 167.65, 164.26, 163.59, 157.89, 150.84, 136.19, 132.34, 131.69, 130.08, 128.66, 127.53, 115.27, 114.85, 101.50, 67.55, 65.97, 56.20, 48.73, 41.77, 41.45, 36.99.

HRMS (ESI): calculated for $[C_{30}H_{32}N_4O_6S + H]^+$ = 577.2115, found 577.2109

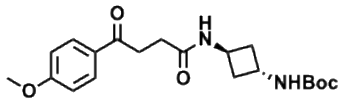

EL-1-013

Synthesized using General Procedure A, with 4-(4-methoxyphenyl)-4-oxobutanoic acid (100.0 mg, 0.480 mmol), tert-Butyl (trans-3-aminocyclobutyl)carbamate (98.40 mg, 0.528 mmol), HATU (365.24 mg, 0.961 mmol) and DIPEA (0.256 mL, 1.44 mmol). The crude residue was purified by silica gel chromatography (5 – 80% EtOAC in hexanes) to afford 33.20 mg of the title compound (18.36%) as a white solid.

^{1}H NMR (400 MHz, DMSO-D6) δ 8.16 (d, J = 7.0 Hz, 1H), 7.94 – 7.86 (m, 2H), 7.17 (d, J = 7.4 Hz, 1H), 7.03 – 6.96 (m, 2H), 4.08 (h, J = 6.6 Hz, 1H), 4.03 – 3.92 (m, 1H), 3.80 (s, 3H), 3.12 (t, J = 6.7 Hz, 2H), 2.38 (t, J = 6.7 Hz, 2H), 2.13 – 2.01 (m, 4H), 1.33 (s, 9H).

^{13}C NMR (101 MHz, DMSO-D6) δ 197.79, 171.27, 163.56, 155.34, 130.67, 114.37, 78.10, 56.04, 42.68, 41.10, 40.75, 40.70, 40.54, 40.49, 40.33, 40.28, 40.07, 39.86, 39.65, 39.45, 37.32, 33.47, 29.82, 28.78.

HRMS: calculated for $[C_{20}H_{28}N_2O_5 + H]^+$ = 376.1998, found 376.1987

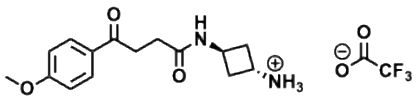

EL-1-014

Synthesized using General Procedure C.

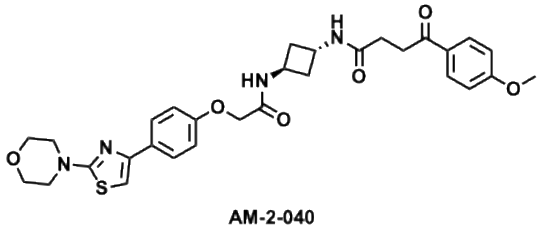

AM-2-040

Synthesized using General Procedure A, with **EL-1-014** (22.63 mg, 0.045 mmol), 4-(4-methoxyphenyl)-4-oxobutanoic acid (10.31 mg, 0.050 mmol), HATU (51.37 mg, 0.135

mmol), DIPEA (0.032 mL, 0.181 mmol). The crude residue was purified by silica gel chromatography (0-10% MeOH in DCM) to afford 14.2 mg of the title compound (54.5%) as an orange solid.

^{1}H NMR (500 MHz, DMSO) δ 8.51 (d, *J* = 7.5 Hz, 1H), 8.35 (d, *J* = 7.1 Hz, 1H), 8.03 – 7.98 (m, 2H), 7.88 – 7.82 (m, 2H), 7.21 (s, 1H), 7.12 – 7.07 (m, 2H), 7.06 – 7.00 (m, 2H), 4.54 (s, 2H), 4.49 – 4.40 (m, 1H), 4.28 (tq, *J* = 7.6, 3.9 Hz, 1H), 3.90 (s, 3H), 3.82 – 3.76 (m, 4H), 3.49 (dd, *J* = 5.9, 3.8 Hz, 4H), 3.23 (t, *J* = 6.8 Hz, 2H), 2.49 (t, *J* = 6.7 Hz, 2H), 2.33 (ddd, *J* = 11.0, 8.2, 5.7 Hz, 2H), 2.23 (ddd, *J* = 12.5, 8.0, 5.0 Hz, 2H).

^{13}C NMR (126 MHz, DMSO) δ 197.71, 171.28, 171.15, 167.51, 163.49, 157.81, 150.76, 130.61, 130.02, 128.56, 127.44, 115.17, 115.02, 114.30, 101.51, 101.42, 67.44, 65.90, 55.98, 48.65, 41.35, 41.30, 41.26, 41.21, 40.57, 40.48, 40.41, 40.32, 40.24, 40.15, 40.07, 39.98, 39.90, 39.82, 39.65, 39.48, 37.09, 37.03, 33.41, 29.76.

HRMS (ESI): calculated for $[C_{30}H_{34}N_4O_6S + H]^+$ = 579.2272, found 579.2264

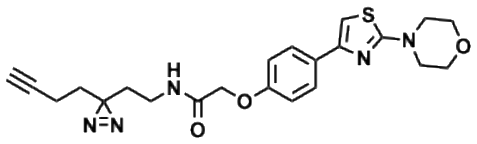

VPC-14228 PAL probe

Synthesized using General Procedure A, with tert-butyl 2-(4-(2-morpholinothiazol-4-yl)phenoxy)acetate (10 mg, 0.031 mmol), 2-(3-(but-3-yn-1-yl)-3*H*-diazirin-3-yl)ethan-1-amine (4.7 mg, 0.034 mmol), HATU (11.87 mg, 0.031 mmol), and DIPEA (0.022 mL, 0.125 mmol). The crude residue was purified by silica gel chromatography (0-10% MeOH in DCM) to afford 8.0 mg (58.5%) of the title compound as a beige solid.

^{1}H NMR (400 MHz, DMSO-D_6) δ 8.06 (t, *J* = 5.6 Hz, 1H), 7.78 – 7.72 (m, 2H), 7.11 (s, 1H), 6.97 – 6.90 (m, 2H), 4.45 (s, 2H), 3.69 (t, *J* = 4.9 Hz, 4H), 3.39 (t, *J* = 4.9 Hz, 4H), 3.01 (q, *J* = 6.8 Hz, 2H), 2.79 (t, *J* = 2.6 Hz, 1H), 1.95 (td, *J* = 7.4, 2.6 Hz, 2H), 1.54 (dt, *J* = 9.6, 7.3 Hz, 4H).

^{13}C NMR (101 MHz, DMSO-D_6) δ 168.12, 157.76, 150.81, 127.54, 115.30, 72.32, 65.97, 48.72, 31.78, 27.69, 13.21.

HRMS (ESI): calculated for $[C_{22}H_{25}N_5O_3S + H]^+$ = 440.1751, found 440.1743

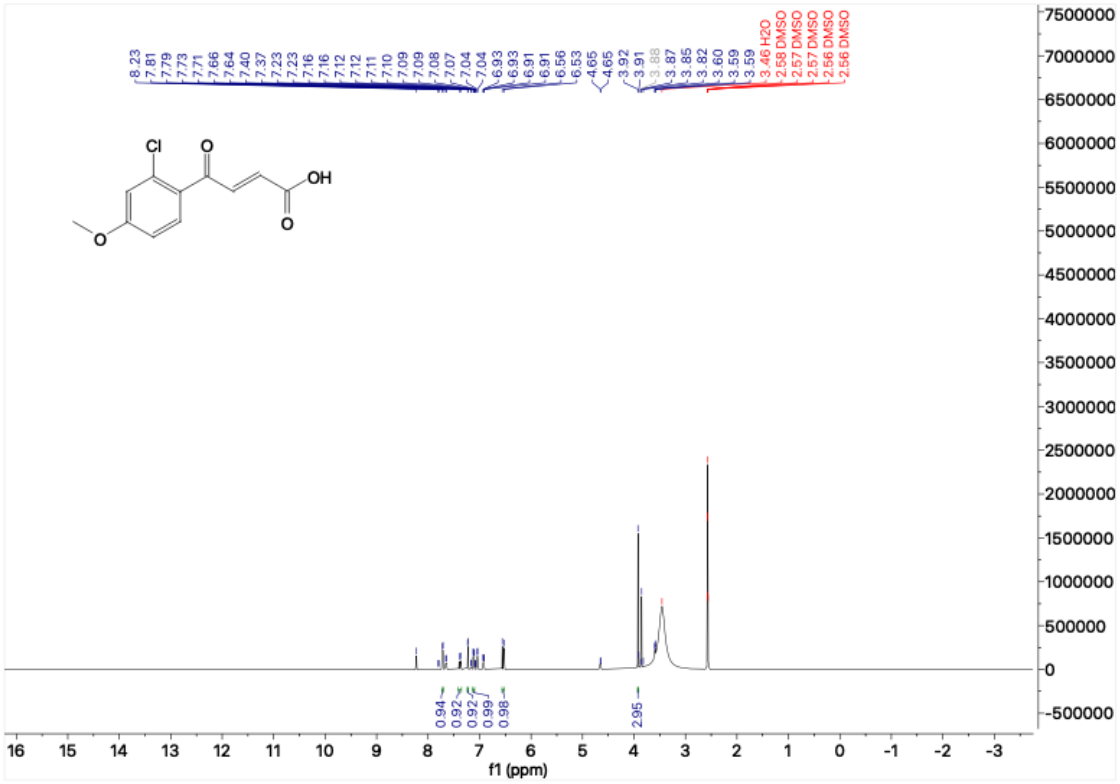
8.23
7.81
7.79
7.73
7.71
7.66
7.64
7.40
7.37
7.23
7.23
7.16
7.16
7.12
7.12
7.11
7.10
7.09
7.09
7.08
7.07
7.04
7.04
6.93
6.93
6.91
6.91
6.56
6.53
4.65
4.65
3.92
3.91
3.88
3.87
3.85
3.82
3.60
3.59
3.59
3.46 H2O
2.58 DMSO
2.57 DMSO
2.57 DMSO
2.56 DMSO
2.56 DMSO
Cl
O
OH
O
O
0.94
0.92
0.92
0.99
0.98
2.95
f1 (ppm)

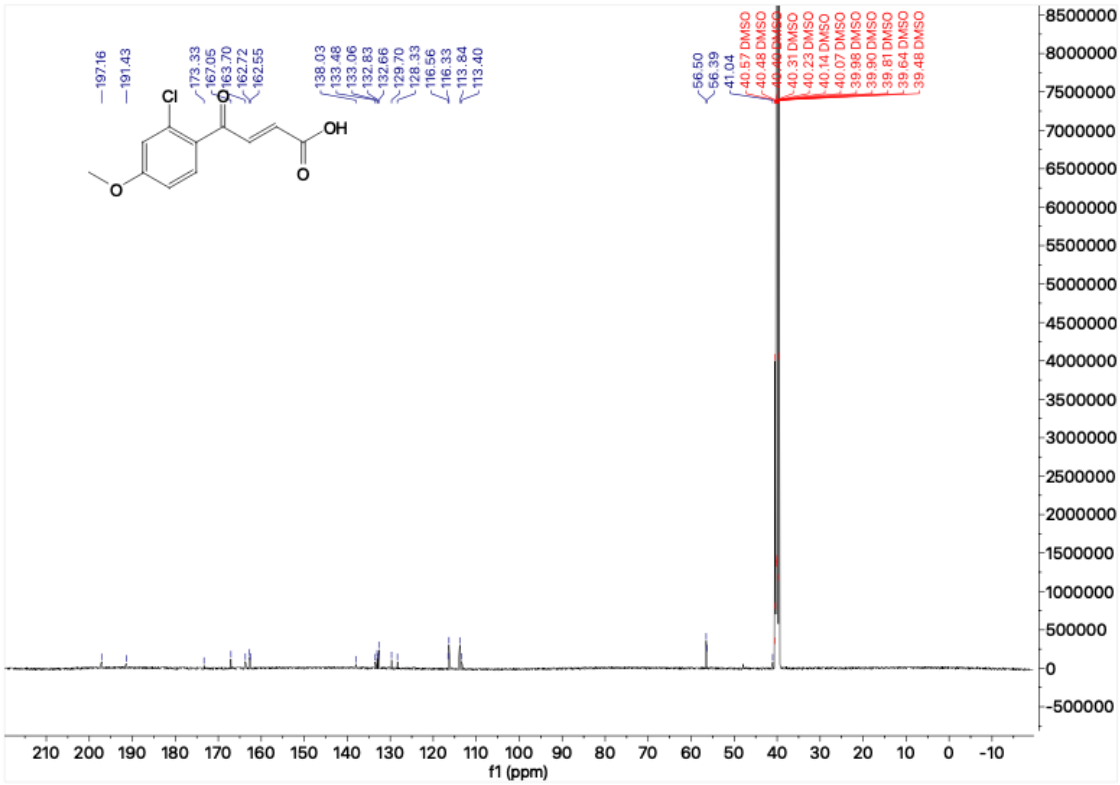
197.16
191.43
173.33
167.05
163.70
162.72
162.55
138.03
133.48
133.06
132.83
132.66
129.70
128.33
116.56
116.33
113.84
113.40
56.50
56.39
41.04
40.57 DMSO
40.48 DMSO
40.40 DMSO
40.31 DMSO
40.23 DMSO
40.14 DMSO
40.07 DMSO
39.98 DMSO
39.90 DMSO
39.81 DMSO
39.64 DMSO
39.48 DMSO
Cl
O
OH
O
O
f1 (ppm)

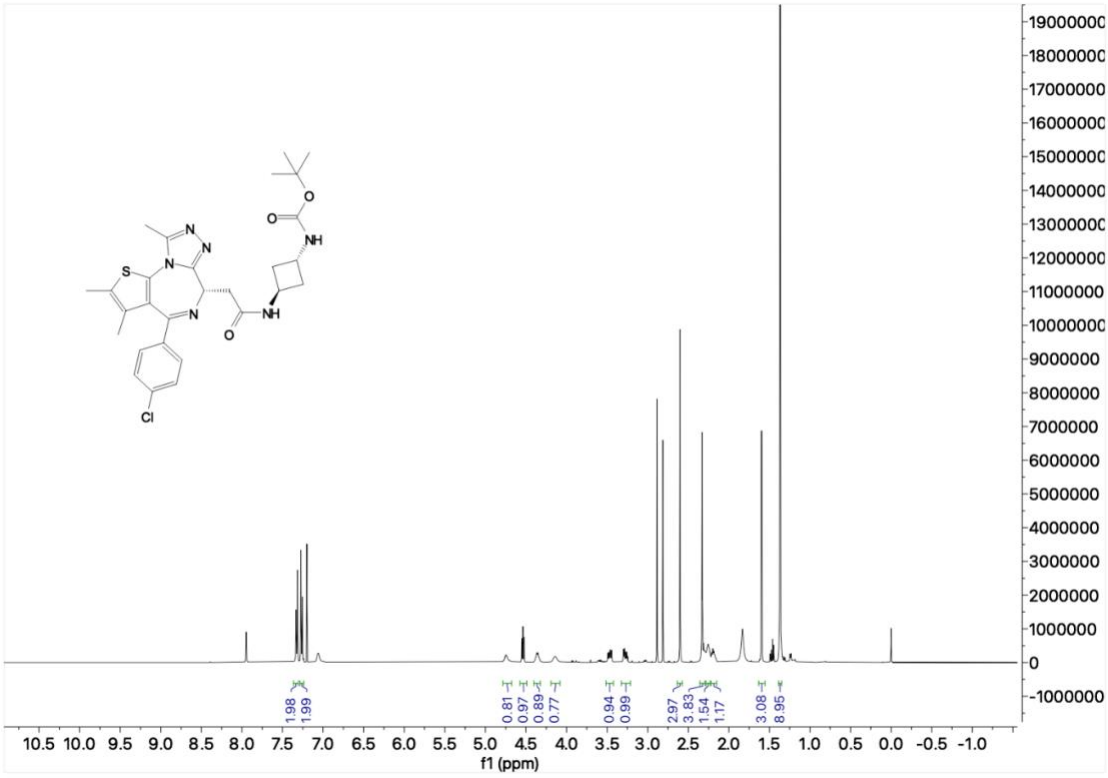
1.98
1.99
0.81
0.97
0.89
0.77
0.94
0.99
2.97
3.83
1.54
1.17
3.08
8.95
f1 (ppm)

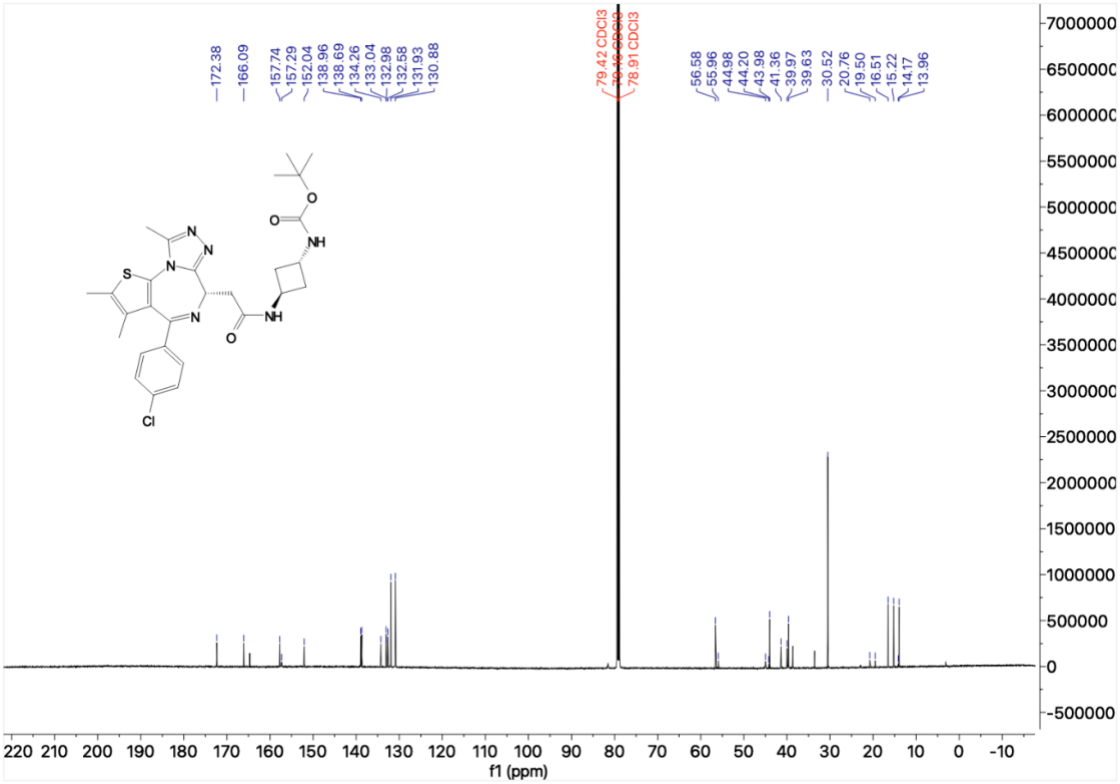
172.38
166.09
157.74
157.29
152.04
138.96
138.69
134.26
133.04
132.98
132.58
131.93
130.88
79.42 CDCl3
78.16 CDCl3
78.91 CDCl3
56.58
55.96
44.98
44.20
43.98
41.36
39.97
39.63
30.52
20.76
19.50
16.51
15.22
14.17
13.96
f1 (ppm)

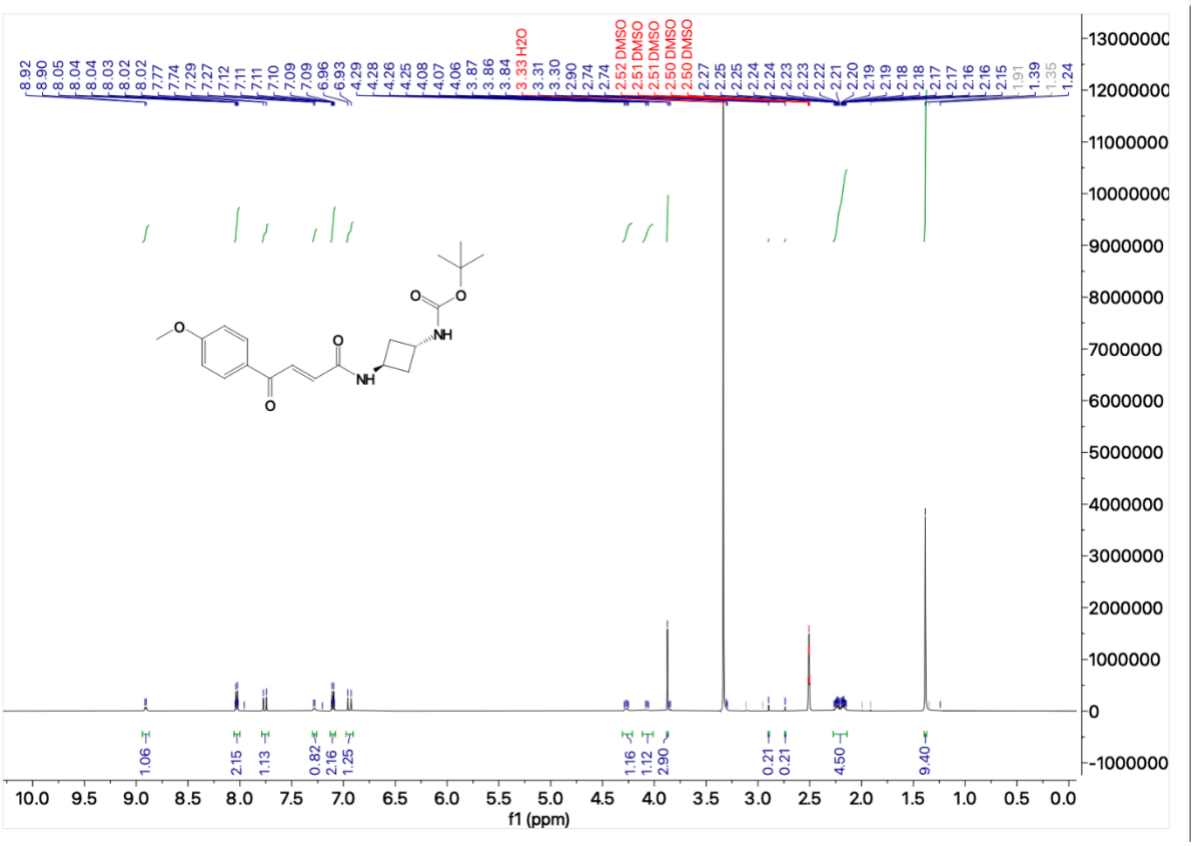
8.92 8.90 8.05 8.04 8.04 8.03 8.02 8.02 7.77 7.74 7.29 7.27 7.12 7.11 7.11 7.10 7.09 7.09 6.96 6.93 4.29 4.28 4.26 4.25 4.08 4.07 4.06 3.87 3.86 3.84 3.33 H2O 3.31 3.30 2.90 2.74 2.74 2.52 DMSO 2.51 DMSO 2.51 DMSO 2.50 DMSO 2.50 DMSO 2.27 2.25 2.25 2.24 2.24 2.23 2.23 2.22 2.21 2.20 2.19 2.19 2.18 2.18 2.17 2.17 2.16 2.16 2.15 1.91 1.39 1.35 1.24
1.06 2.15 1.13 0.82 2.16 1.25 1.16 1.12 2.90 0.21 0.21 4.50 9.40
f1 (ppm)

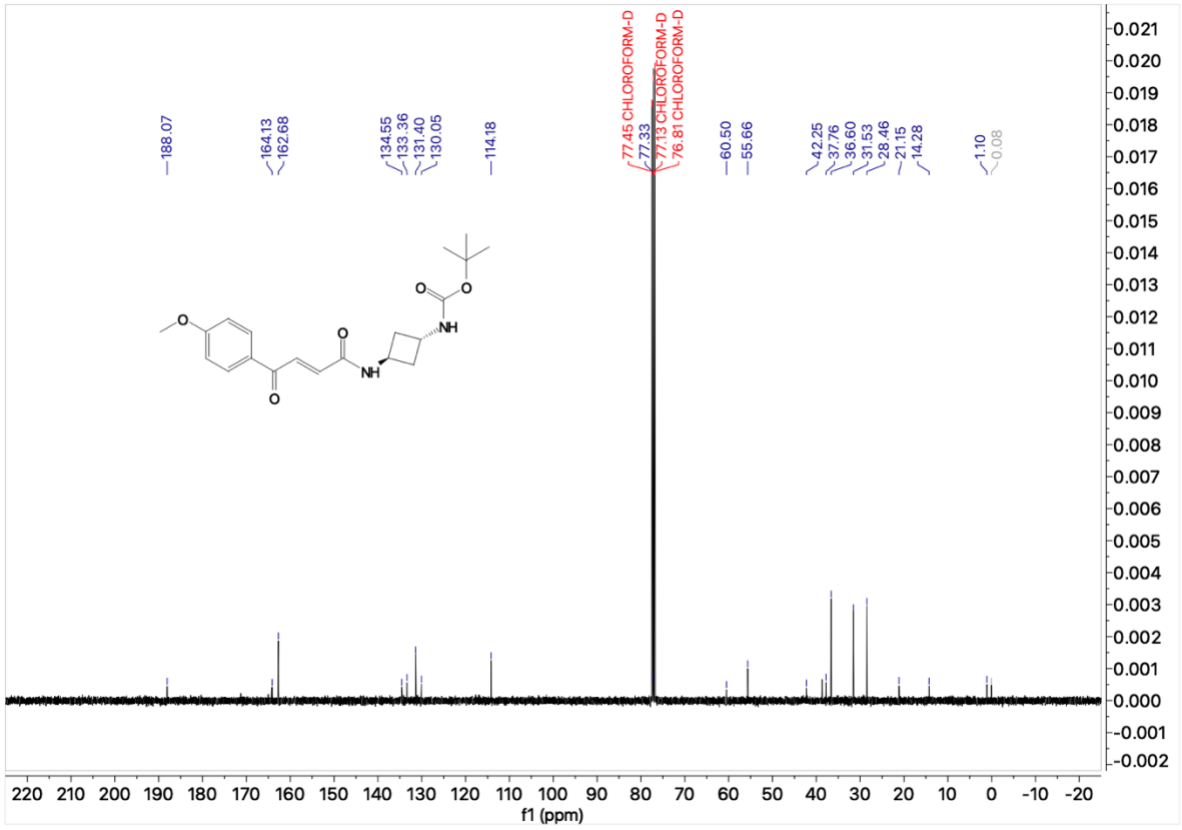
188.07 164.13 162.68 134.55 133.36 131.40 130.05 114.18 77.45 CHLOROFORM-D 77.33 77.13 CHLOROFORM-D 76.81 CHLOROFORM-D 60.50 55.66 42.25 37.76 36.60 31.53 28.46 21.15 14.28 1.10 0.08
f1 (ppm)

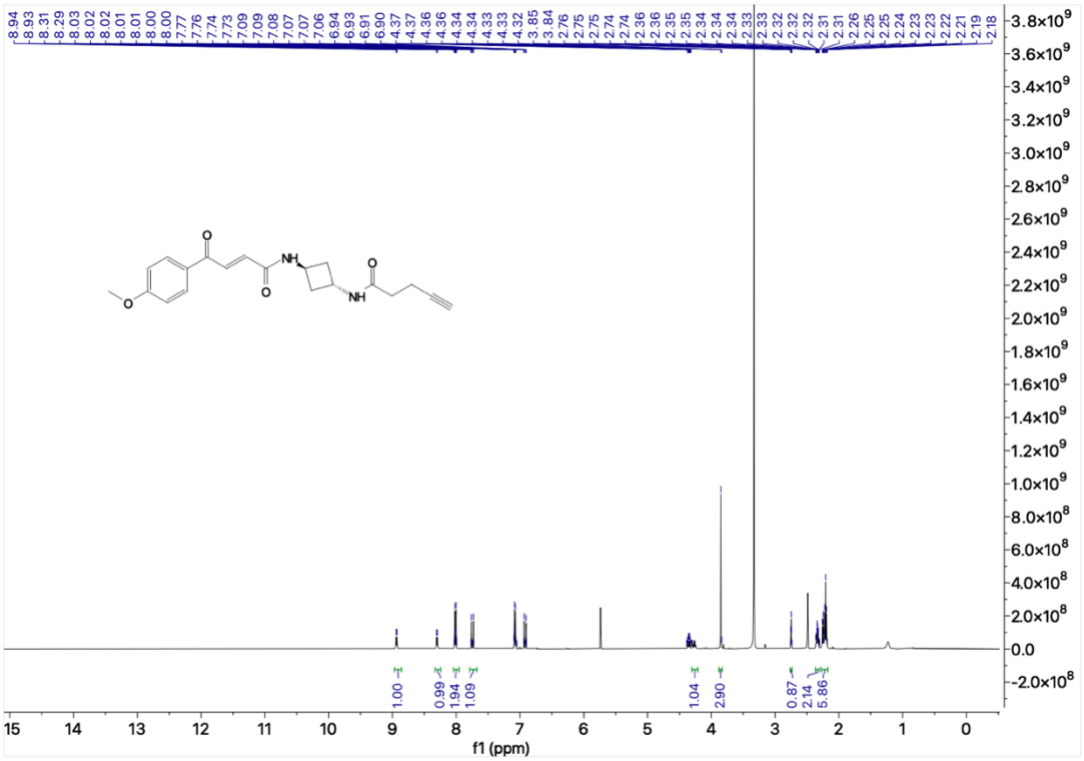
f1 (ppm)

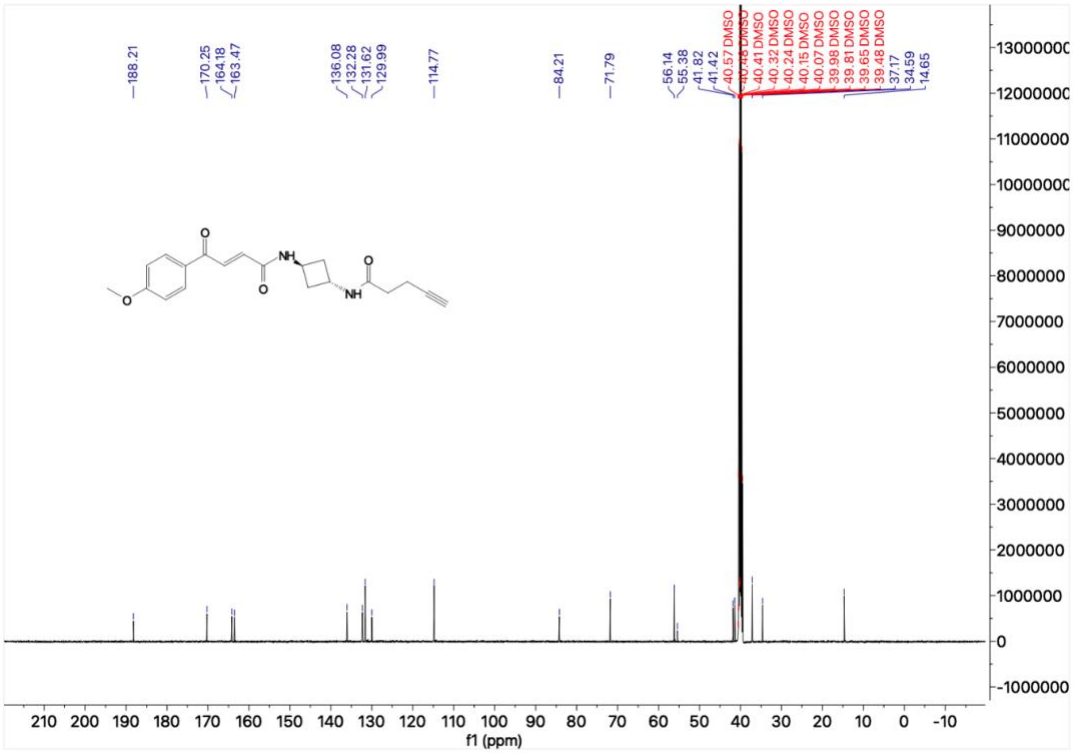
f1 (ppm)

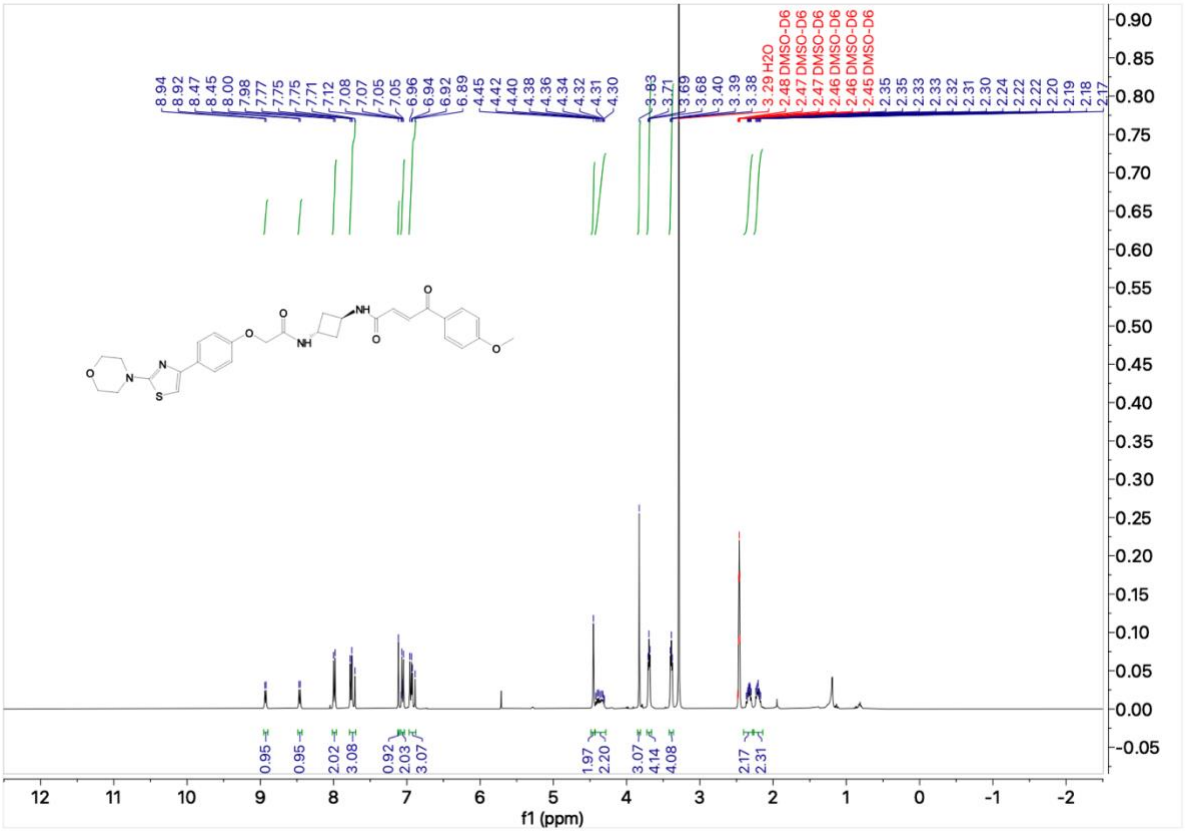
8.94
8.92
8.47
8.45
8.00
7.98
7.77
7.75
7.75
7.71
7.12
7.08
7.07
7.05
7.05
6.96
6.94
6.92
6.89
4.45
4.42
4.40
4.38
4.36
4.34
4.32
4.31
4.30
3.83
3.71
3.69
3.68
3.40
3.39
3.38
3.29 H2O
2.48 DMSO-D6
2.47 DMSO-D6
2.47 DMSO-D6
2.46 DMSO-D6
2.46 DMSO-D6
2.45 DMSO-D6
2.35
2.35
2.33
2.33
2.32
2.31
2.30
2.24
2.22
2.22
2.20
2.19
2.18
2.17
0.95
0.95
2.02
3.08
0.92
2.03
3.07
1.97
2.20
3.07
4.14
4.08
2.17
2.31
f1 (ppm)

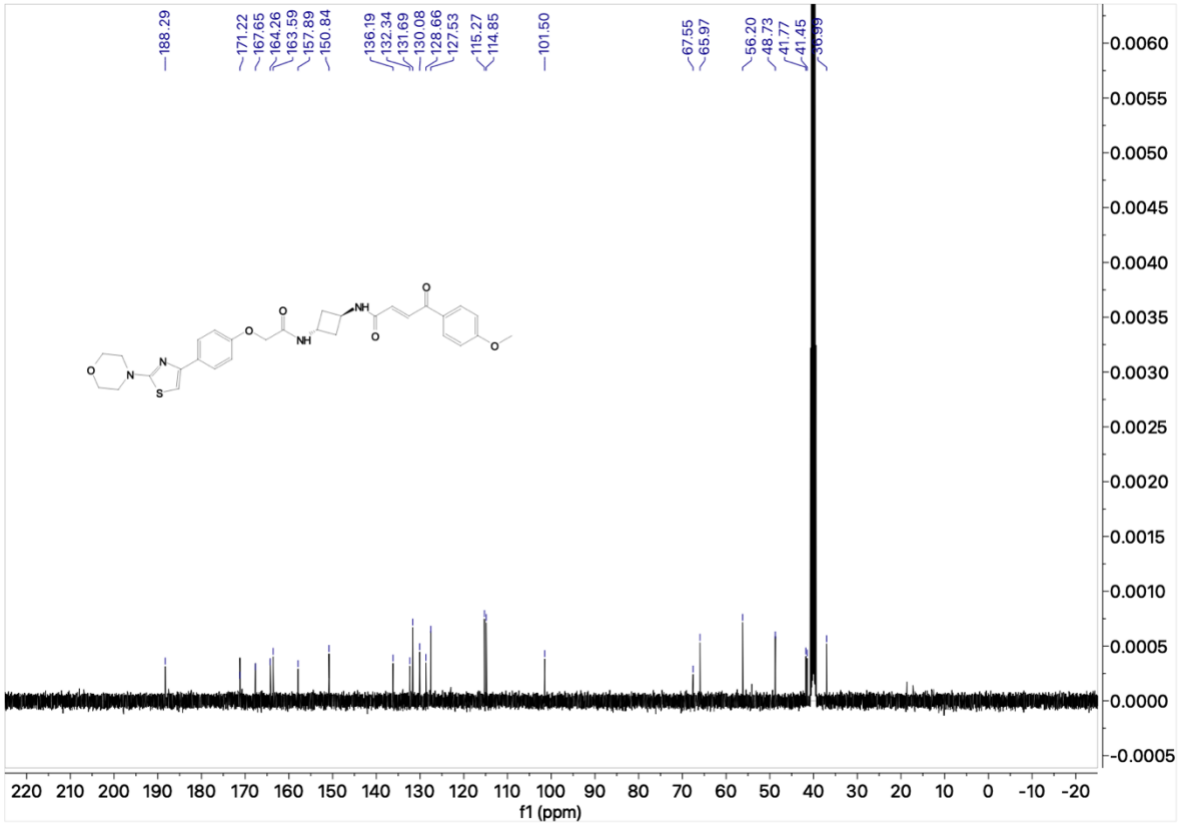
188.29
171.22
167.65
164.26
163.59
157.89
150.84
136.19
132.34
131.69
130.08
128.66
127.53
115.27
114.85
101.50
67.55
65.97
56.20
48.73
41.77
41.45
30.99
f1 (ppm)

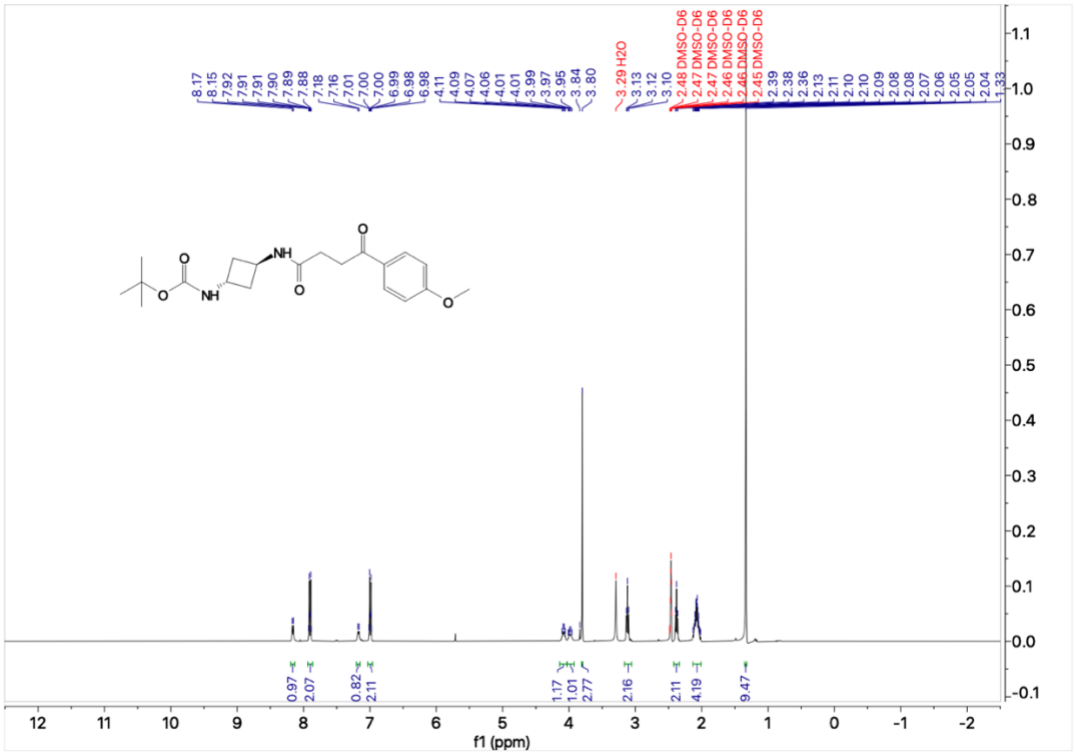
8.17
8.15
7.92
7.91
7.91
7.90
7.89
7.88
7.18
7.16
7.01
7.00
7.00
6.99
6.98
6.98
4.11
4.09
4.07
4.06
4.01
4.01
3.99
3.97
3.95
3.84
3.80
3.29 H2O
3.13
3.12
3.10
2.48 DMSO-D6
2.47 DMSO-D6
2.47 DMSO-D6
2.46 DMSO-D6
2.46 DMSO-D6
2.45 DMSO-D6
2.39
2.38
2.36
2.13
2.11
2.10
2.10
2.09
2.08
2.08
2.07
2.06
2.05
2.05
2.04
1.33
0.97
2.07
0.82
2.11
1.17
1.01
2.77
2.16
2.11
4.19
9.47
f1 (ppm)

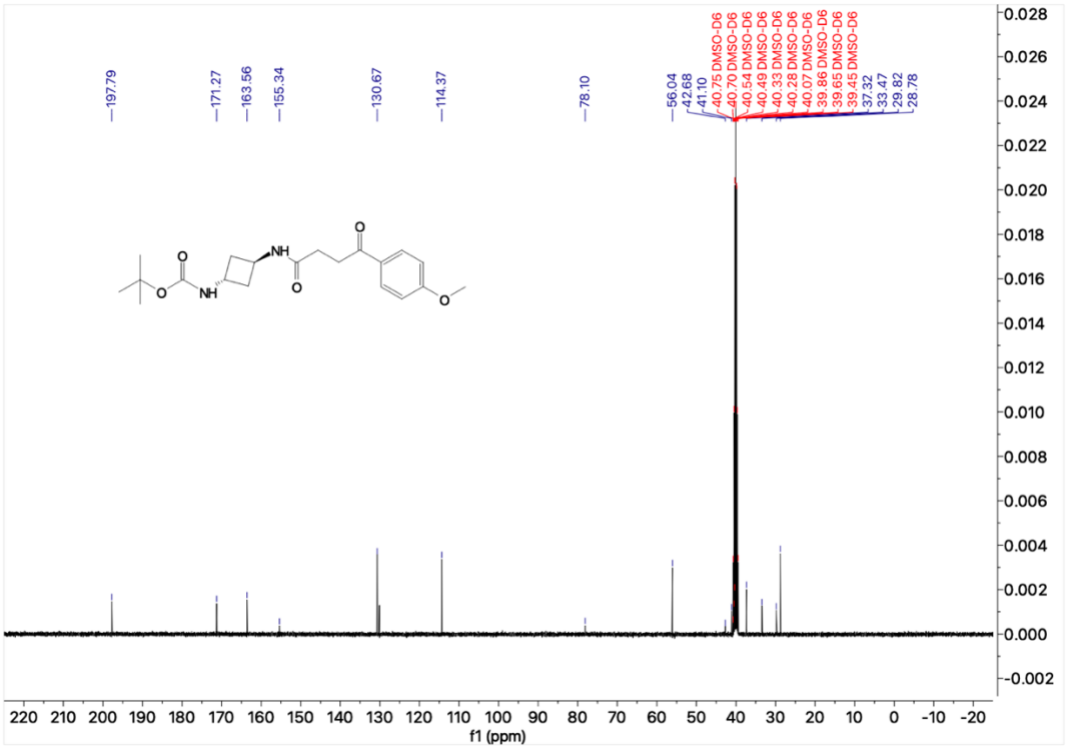
197.79
171.27
163.56
155.34
130.67
114.37
78.10
56.04
42.68
41.10
40.75 DMSO-D6
40.70 DMSO-D6
40.54 DMSO-D6
40.49 DMSO-D6
40.33 DMSO-D6
40.28 DMSO-D6
40.07 DMSO-D6
39.86 DMSO-D6
39.65 DMSO-D6
39.45 DMSO-D6
37.32
33.47
29.82
28.78
f1 (ppm)

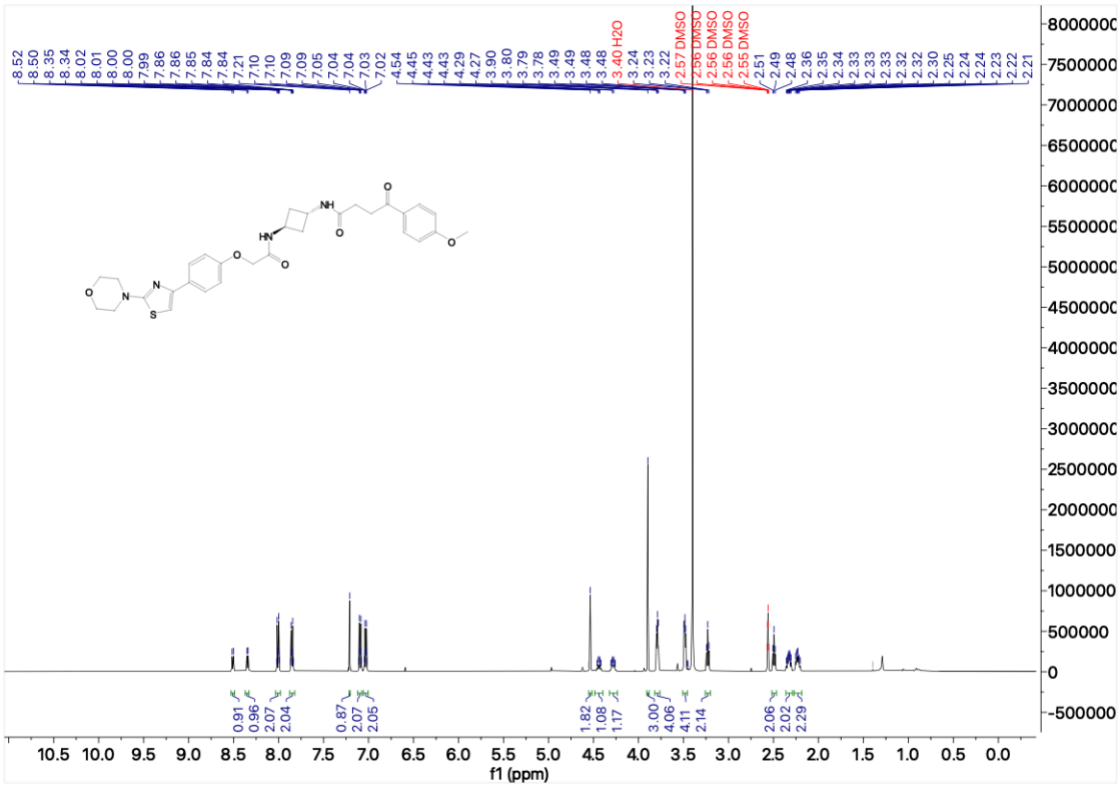
8.52
8.50
8.35
8.34
8.02
8.01
8.00
8.00
7.99
7.86
7.86
7.85
7.84
7.84
7.21
7.10
7.10
7.09
7.09
7.05
7.04
7.04
7.03
7.02
4.54
4.45
4.43
4.43
4.29
4.27
3.90
3.80
3.79
3.78
3.49
3.49
3.48
3.48
3.40 H2O
3.24
3.23
3.22
2.57 DMSO
2.56 DMSO
2.56 DMSO
2.55 DMSO
2.51
2.49
2.48
2.36
2.35
2.34
2.33
2.33
2.33
2.32
2.32
2.30
2.25
2.24
2.24
2.23
2.22
2.21
0.91
0.96
2.07
2.04
0.87
2.07
2.05
1.82
1.08
1.17
3.00
4.06
4.11
2.14
2.06
2.02
2.29
f1 (ppm)

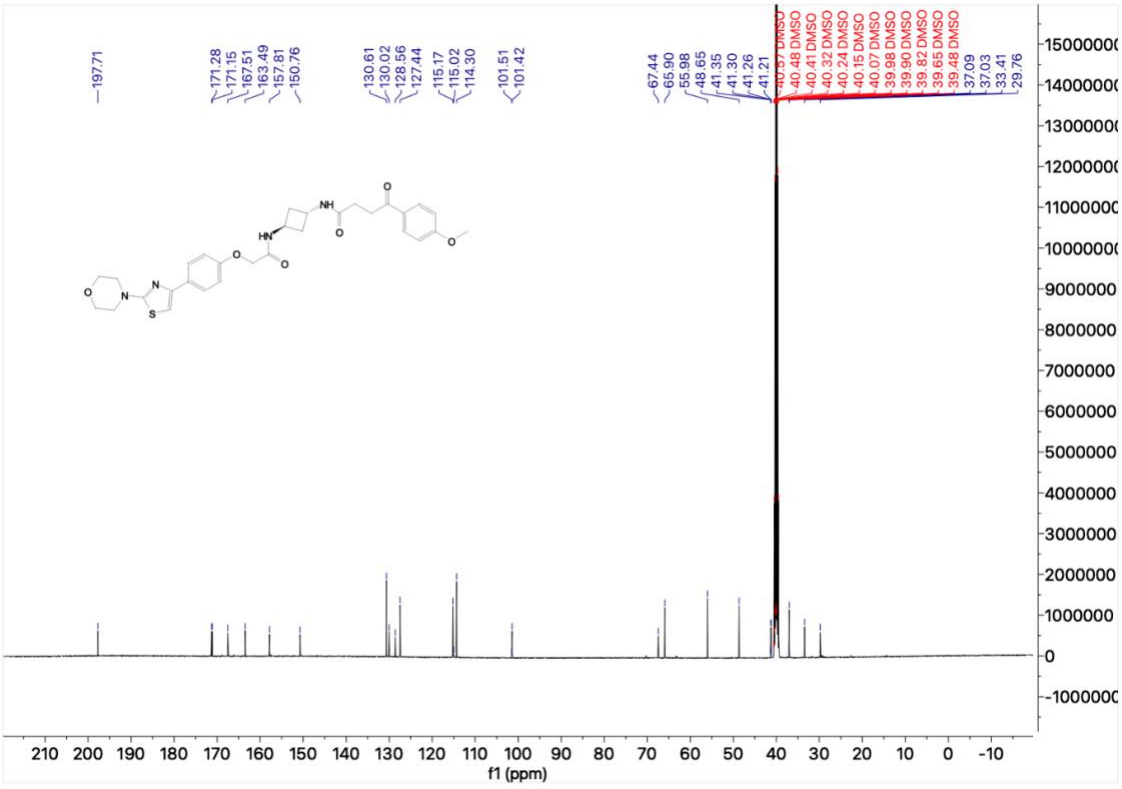
197.71
171.28
171.15
167.51
163.49
157.81
150.76
130.61
130.02
128.56
127.44
115.17
115.02
114.30
101.51
101.42
67.44
65.90
55.98
48.65
41.35
41.30
41.26
41.21
40.57 DMSO
40.48 DMSO
40.41 DMSO
40.32 DMSO
40.24 DMSO
40.15 DMSO
40.07 DMSO
39.98 DMSO
39.90 DMSO
39.82 DMSO
39.65 DMSO
39.48 DMSO
37.09
37.03
33.41
29.76
f1 (ppm)

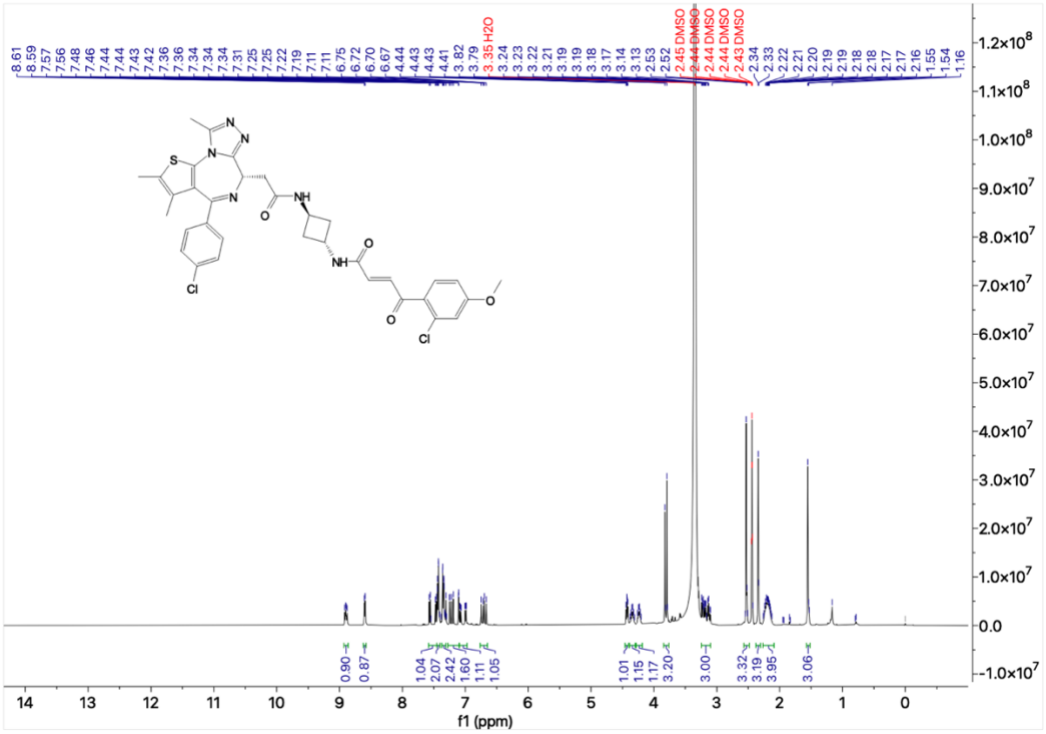
8.61
8.59
7.57
7.56
7.48
7.46
7.44
7.44
7.43
7.42
7.36
7.36
7.34
7.34
7.34
7.31
7.25
7.25
7.22
7.19
7.11
7.11
6.75
6.72
6.70
6.67
4.44
4.43
4.43
4.41
3.82
3.79
3.35 H2O
3.24
3.23
3.22
3.21
3.19
3.19
3.18
3.17
3.14
3.13
2.53
2.52
2.45 DMSO
2.44 DMSO
2.44 DMSO
2.44 DMSO
2.43 DMSO
2.34
2.33
2.22
2.21
2.20
2.19
2.19
2.18
2.18
2.17
2.17
2.16
1.55
1.54
1.16
0.90
0.87
1.04
2.07
2.42
1.60
1.11
1.05
1.01
1.15
1.17
3.20
3.00
3.32
3.19
3.95
3.06
f1 (ppm)

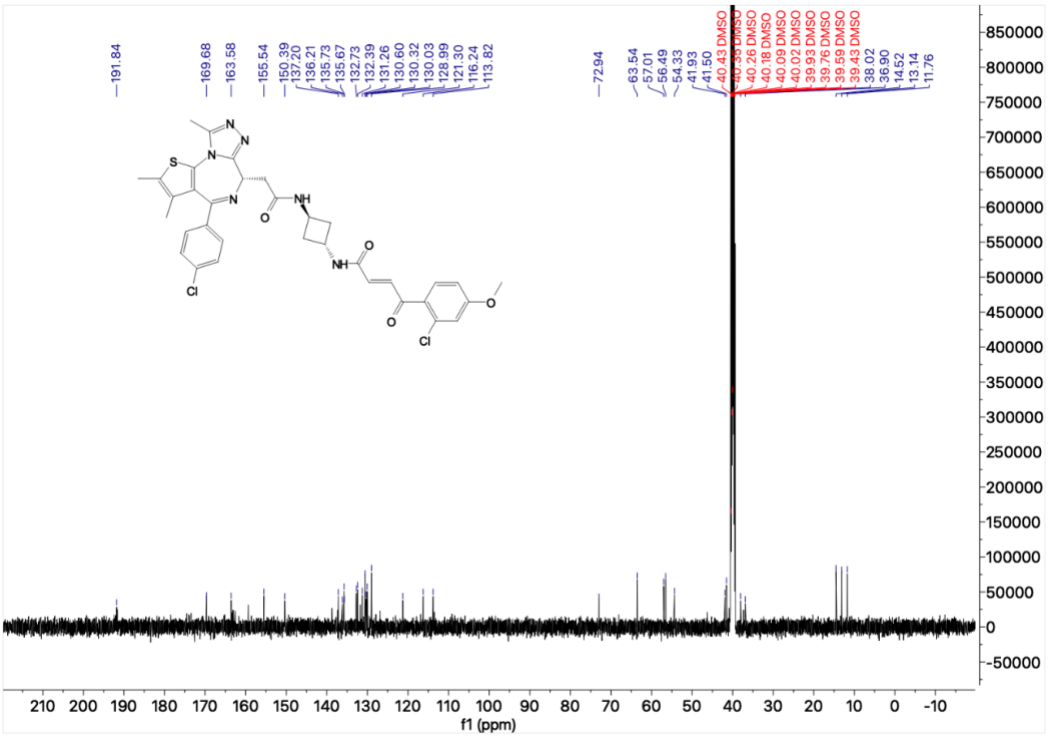
191.84
169.68
163.58
155.54
150.39
137.20
136.21
135.73
135.67
132.73
132.39
131.26
130.60
130.32
130.03
128.99
121.30
116.24
113.82
72.94
63.54
57.01
56.49
54.33
41.93
41.50
40.43 DMSO
40.35 DMSO
40.26 DMSO
40.18 DMSO
40.09 DMSO
40.02 DMSO
39.93 DMSO
39.76 DMSO
39.59 DMSO
39.43 DMSO
38.02
36.90
14.52
13.14
11.76
f1 (ppm)

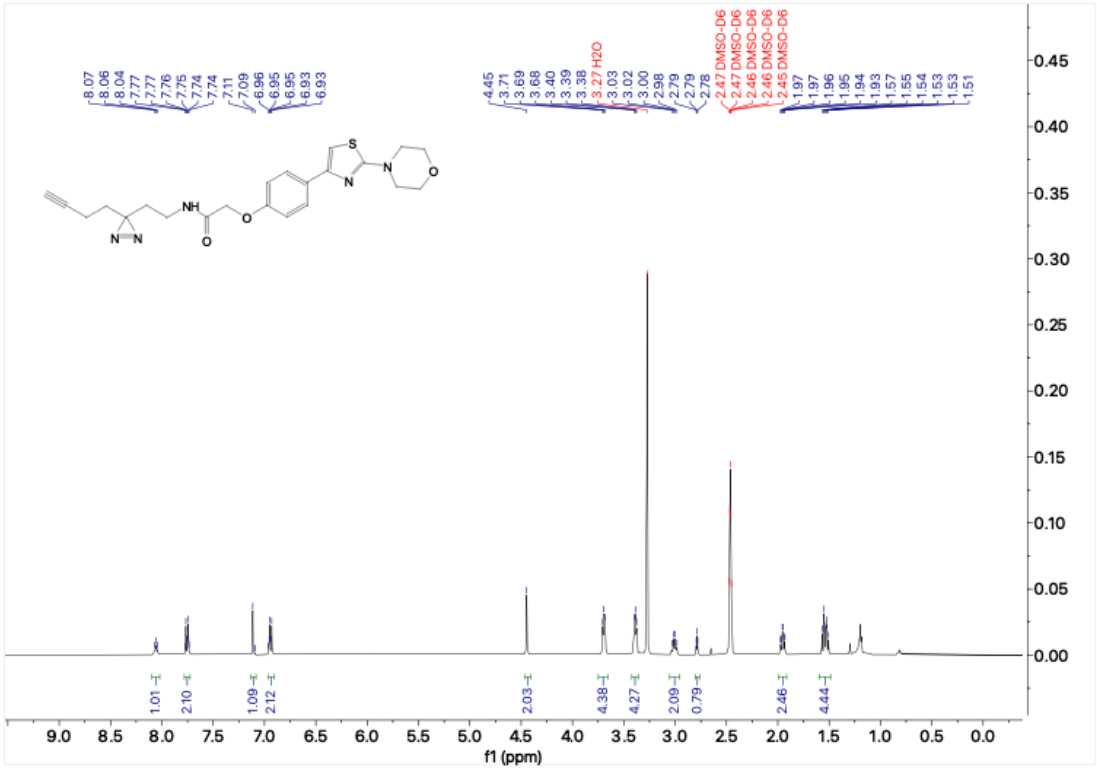
8.07
8.06
8.04
7.77
7.77
7.76
7.75
7.74
7.74
7.11
7.09
6.96
6.95
6.95
6.93
6.93
4.45
3.71
3.69
3.68
3.40
3.39
3.38
3.27 H2O
3.03
3.02
3.00
2.98
2.79
2.79
2.78
2.47 DMSO-D6
2.47 DMSO-D6
2.46 DMSO-D6
2.46 DMSO-D6
2.45 DMSO-D6
1.97
1.97
1.96
1.95
1.94
1.93
1.57
1.55
1.54
1.53
1.53
1.51
1.01
2.10
1.09
2.12
2.03
4.38
4.27
2.09
0.79
2.46
4.44
f1 (ppm)

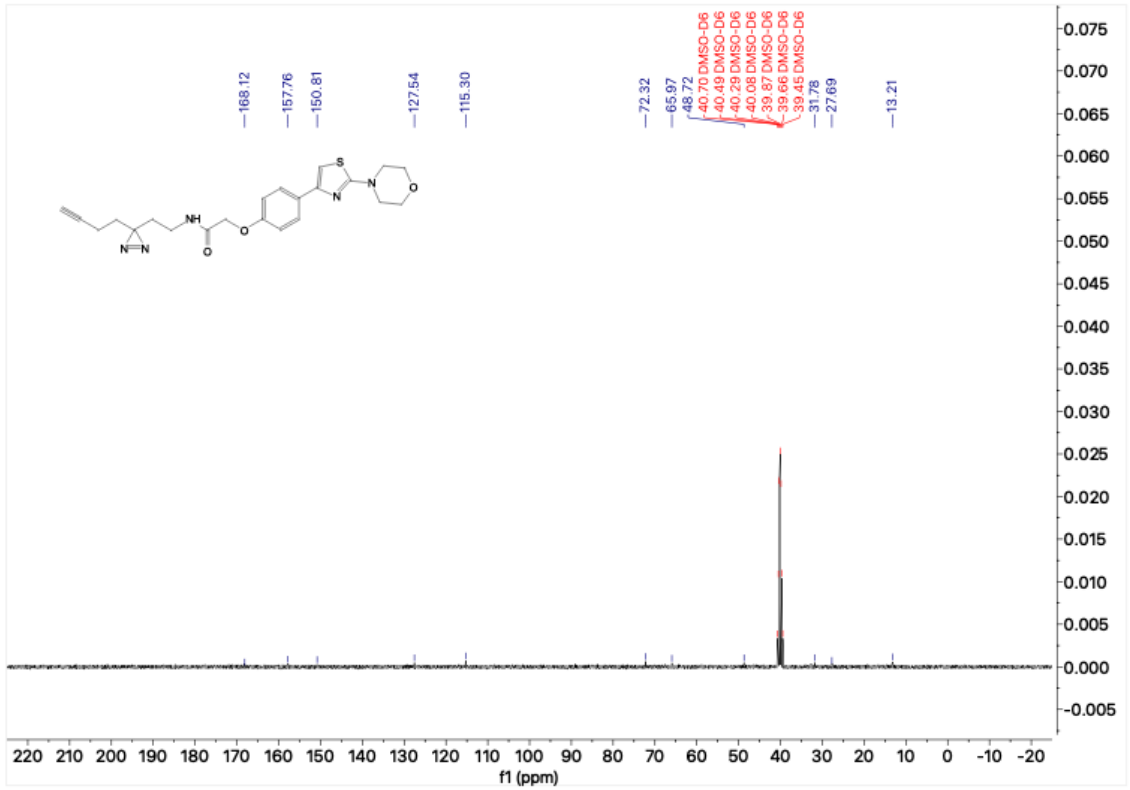
168.12
157.76
150.81
127.54
115.30
72.32
65.97
48.72
40.70 DMSO-D6
40.49 DMSO-D6
40.29 DMSO-D6
40.08 DMSO-D6
39.87 DMSO-D6
39.66 DMSO-D6
39.45 DMSO-D6
31.78
27.69
13.21
f1 (ppm)

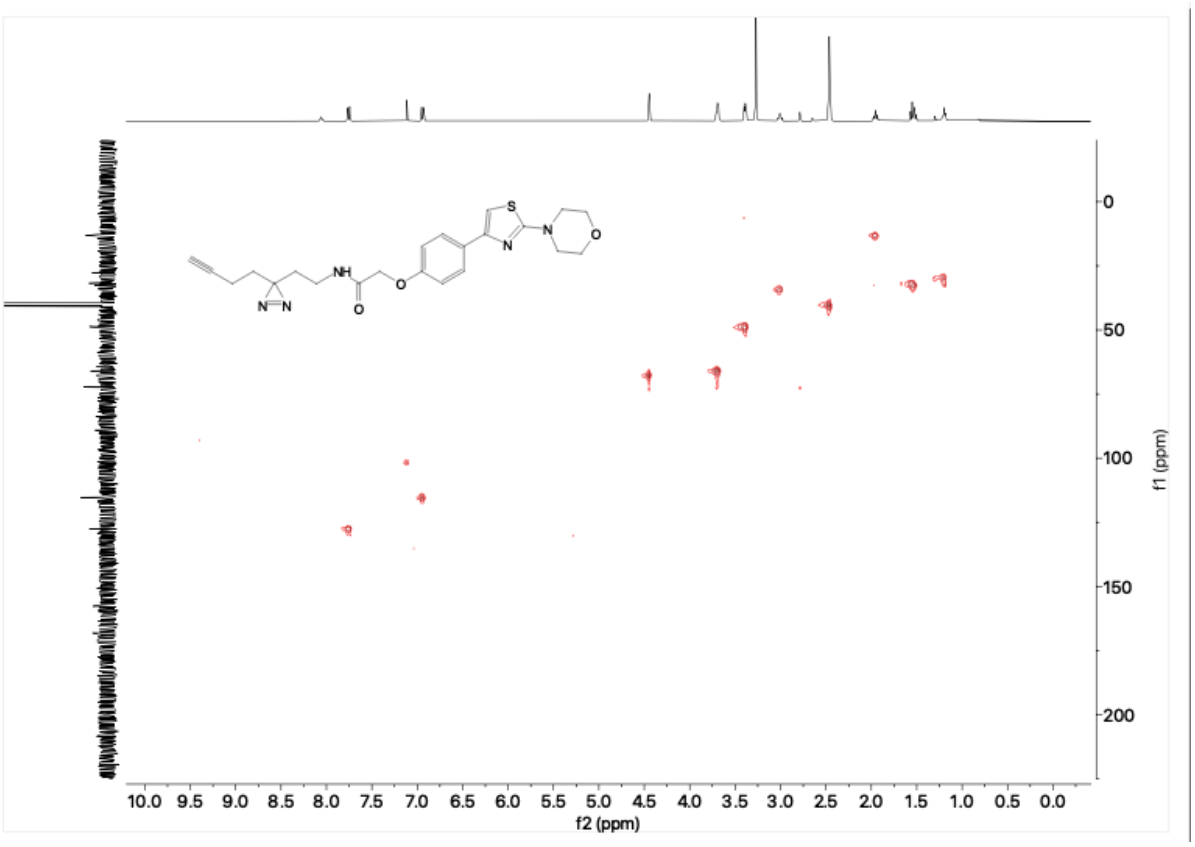
S
N
O
NH
O
N
N
0
50
100
150
200
f1 (ppm)
10.0 9.5 9.0 8.5 8.0 7.5 7.0 6.5 6.0 5.5 5.0 4.5 4.0 3.5 3.0 2.5 2.0 1.5 1.0 0.5 0.0
f2 (ppm)